Numerical Modelling of Non-ideal Catalytic Systems

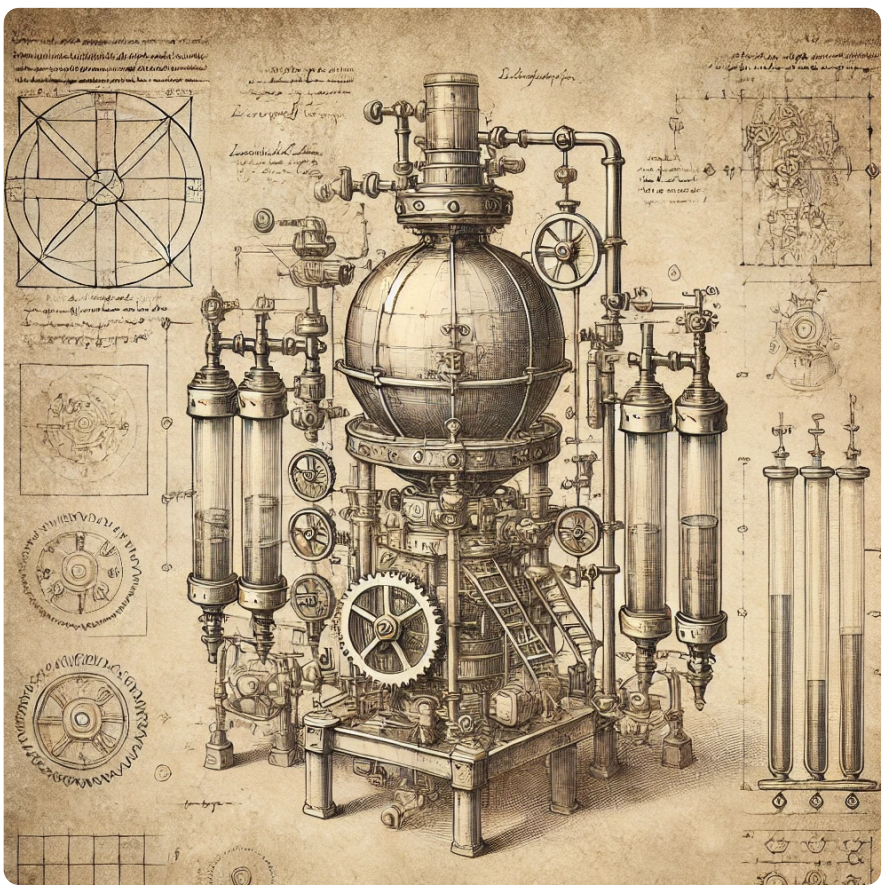

Ivo Filot

“Nanos gigantum humeris insidentes.”

Isaac Newton

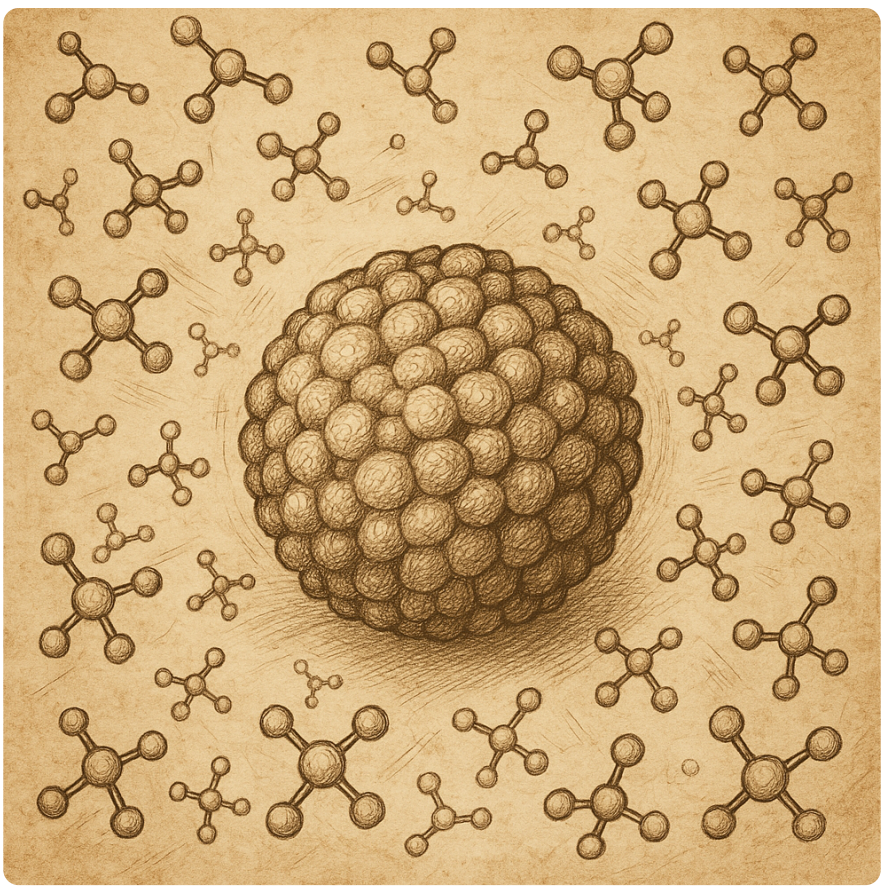

This book was carefully produced. Nevertheless, author and publisher do not warrant the information contained therein to be free of errors. Readers are advised to keep in mind that statements, data, illustrations, procedural details or other items may inadvertently be inaccurate.

Filot, I.A.W.
Numerical Modelling of Non-ideal Catalytic Systems
Eindhoven University of Technology

Subject headings: finite volume method, reactor engineering, catalysis, reaction, diffusion, convection

Version 1.3.0

Git commit id: d41d0c
Commit date: October 24, 2025
Compile date: October 24, 2025

.

ELECTRONIC LECTURE MATERIAL

Electronic lecture material associated with this book can be obtained, free of charge, at: https://ifilot.pages.tue.nl/numerical-modelling-of-non-ideal-catalytic-systems/

.

ACKNOWLEDGEMENTS

This book would not have been possible without the support and contributions of many individuals, to whom I am deeply grateful. I would like to sincerely acknowledge their invaluable assistance, guidance, and encouragement throughout this journey. Their insights, feedback, and unwavering belief in my work have been instrumental in bringing this project to completion.

I would like to express my sincere gratitude to John van der Schaaf, Mart de Croon, and Jaap Schouten for their inspirational lectures in the field of chemical reactor engineering. Their expertise, passion, and dedication to the subject have been a continuous source of motivation throughout my work. Although my focus has since shifted to theoretical and computational chemistry at the nanoscale, my appreciation for chemical reactor modelling at the nanoscale remains as strong as ever. Their teachings have not only deepened my understanding of the field but have also inspired me to explore new ideas and approaches within chemical reactor engineering.

I would also like to express my deep appreciation to my fellow teachers in the course "*Catalysis, Science and Technology*": Emiel Hensen, Robert Pestman, and Michel van Etten. Additionally, a special thank you to Fernanda Neira d'Angelo for her valuable contributions to this course in the past. I would also like to acknowledge Damian Broens and Valentin Jestl for their assistance in guiding the self-study sessions.

Last but not least, I wish to mention a number of students who have provided valuable feedback to improve the overall quality and readability of this book:

- **Class of 2022**: Pedro de Carvalho Ferreira
- **Class of 2023**: Ulla Praisa, Jeroen Vennix, Pascal van Wijk
- **Class of 2024**: Joeri van Limpt, Oisín Rutgers Kearns, Mustafa Dogan, David Warrand, Kim de Krijger

CONTENTS

.

I NUMERICAL MODELLING OF CHEMICAL REACTORS

Contents

1.1 Introduction

This chapter is a brief recap of the fundamental principles of chemical reactor engineering. The concepts of a control volume and mole balances are discussed from which governing equations can be derived. In turn, these governing equations act as the starting point for the design of analytical and numerical models. It is demonstrated how a numerical model approximates the analytical solution in the limit of infinitely fine spatial discretization.

1.2 Derivation of governing equations from control volume balances

Numerical modelling of chemical reactors proceeds via the construction of so-called design equations. These design equations can be considered as a (universal) mathematical descriptor of molecular transport and chemical conversion and are typically in the form of an algebraic equation or an ordinary or partial differential equation. To construct a design equation, one starts with the postulation of a mole balance over a hypothetical reactor volume. There are only four ingredients to this mole balance:

1. The amount of species that **enters** the hypothetical volume within a given time frame

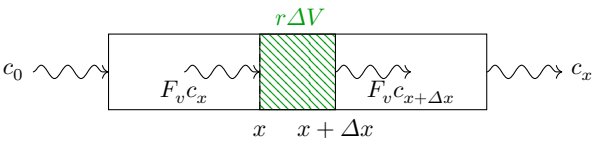

Figure 1.1: *Schematic depiction of the tubular flow reactor.*

2. The amount of species that **leaves** the hypothetical volume within a given time frame
3. The amount of species that is **converted** within the hypothetical volume within a given time frame
4. The **change** of the amount of species within the hypothetical volume within the given time frame

With these four ingredients, we can conceptually construct the following mole balance

$$\{\text{ACCUMULATION}\} = \{\text{IN}\} - \{\text{OUT}\} + \{\text{REACTION}\} \tag{1.1}$$

For each chemical species, one would need to construct a separate mole balance.[1] To demonstrate this principle, we here consider the construction of the design equation for a (tubular) plug-flow reactor. For this reactor set-up, we assume that the chemical flow is uniform throughout the reactor[2] and that there are no gradients in the concentration in the radial direction.

Given a hypothetical volume element inside this reactor (see Figure 1.1), the mole balance would be as follows

$$\dot{N} = (F_v c_x - F_v c_{x+\Delta x} + r\Delta V)\,\Delta t, \tag{1.2}$$

where $\dot{N}$ is the change in the amount of species in the volume element in a certain amount of time Δt, F_v is the volumetric flux (in units of volume per units of time), c_x and $c_{x+\Delta x}$ is the concentration of the species at the left- and right hand side of the hypothetical volume ΔV and r is the volumetric rate of chemical conversion.[3]

By introducing the superficial velocity v, which is defined as the average axial velocity of the medium through the tubular reactor, we can rewrite Equation 1.2 as

$$\dot{N} = (vA_\perp c_x - vA_\perp c_{x+\Delta x} + r\Delta V)\,\Delta t, \tag{1.3}$$

where $A_\perp$ is the surface area perpendicular to the flow direction[4] The change in the amount of species inside the volume can furthermore be written as

[1] This principle can be readily extended to energy, which is also a conserved property. The result is not a mole balance, but a heat or energy balance.

[2] In reality it is not. For example, at the interface of the liquid medium and the reactor wall, the flow is zero.

[3] Which is defined to be negative if the species is a reactant and positive if the species is a product.

[4] Or alternatively, the surface area of the tube.

$$\dot{N} = |c\Delta V|_{t+\Delta t} - |c\Delta V|_t \,. \tag{1.4}$$

At this point, we can introduce two important limits by which we can cast the above equation to a partial differential equation. These two limits are $\Delta t \to 0$ and $\Delta x \to 0$. In other words, the transport and transformation of materials is expressed for an infinitesimally small unit of space and time.

Noting that the superficial velocity v is defined as

$$v = \frac{\partial x}{\partial t} \tag{1.5}$$

and the rate of chemical conversion r is given by

$$r = \frac{\partial c}{\partial t}, \tag{1.6}$$

we can readily cast Equation 1.4 into a partial differential equation by stating that

$$A_\perp \Delta x \lim_{\Delta t \to 0} [c_{t+\Delta t} - c_t] = A_\perp \Delta t \lim_{\Delta x \to 0} [v c_x - v c_{x+\Delta x} + r\Delta x] \tag{1.7}$$

which by division by a factor $A_\perp \Delta x \Delta t$ on both sides of the equation and by application of the definition of the superficial velocity (Equation 1.5) and rate of chemical conversion (Equation 1.6) yields[5]

$$\lim_{\Delta t \to 0} \left[\frac{c_{t+\Delta t} - c_t}{\Delta t}\right] = v \lim_{\Delta x \to 0} \left[\frac{c_x - c_{x+\Delta x}}{\Delta x}\right] + r \tag{1.8}$$

which in turn by application of the fundamental definition of a derivative[6] yields the following partial differential equation[7]

$$\frac{\partial c}{\partial t} = -v\frac{\partial c}{\partial x} + r. \tag{1.9}$$

To solve a partial differential equation, we need to introduce **boundary** conditions and **initial** conditions. The former defines the properties at the boundaries of the spatial domain whereas the latter defines the starting conditions at $t = 0$. For the initial conditions, this would constitute the concentration of the species throughout the reactor at $t = 0$ and for the boundary conditions the concentration right before entering the inlet of the reactor.

One simplification that can be readily applied to solve the partial differential equation is to introduce a steady-state approximation which states that there are no changes in the concentration as function of time. This implies that the left hand side of Equation 1.9 can be set to 0 yielding

$$\frac{\partial c}{\partial x} = \frac{r}{v}. \tag{1.10}$$

[5] Because v and R are already defined in the limit of infinitesimally small time and space, they can be taken outside of the limits.

[6] As you hopefully recall from your Calculus courses.

[7] Admittedly, plenty of the engineering textbooks postulate this partial differential equation, but it is good to see how it can be derived at least once. For the remainder of this lectures notes, I will also simply postulate the governing equation as we have to start from somewhere. Taking things to the extreme, we could start from the Big Bang and work from there, but that is not a very efficient procedure.

[8] I assume here that the species of interest is a reactant.

Next, if we assume that the rate of chemical conversion is given by a first order reaction equation[8]

$$r = -kc, \tag{1.11}$$

then we obtain the following **ordinary** differential equation

$$\frac{dc}{dx} = -\frac{kc}{v}. \tag{1.12}$$

Because Equation 1.12 is a first-order ordinary differential equation, only a single boundary condition is necessary to solve this problem.[9] This single boundary condition corresponds to the concentration c_0 at the inlet of the reactor. Thus, we can cast Equation 1.12 into its integral form as given by

$$\int_{c_0}^{c_x} \frac{dc}{c} = -\int_0^x \frac{k}{v} dx, \tag{1.13}$$

where c_x is the concentration at point x (defined alongside the axial direction) in the reactor. Equation 1.13 is easy enough to directly solve.

$$\int_{c_0}^{c_x} \frac{dc}{c} = -\int_0^x \frac{k}{v} dx \tag{1.14}$$

$$\ln\left(\frac{c_x}{c_0}\right) = -\frac{kx}{v} \tag{1.15}$$

With a little bit of algebra, we can obtain a closed-form expression for the concentration c_x at any axial point in the tubular reactor, which yields

$$c_x = c_0 \exp\left(-\frac{k}{v}x\right). \tag{1.16}$$

Note that the quotient $\frac{x}{v}$ in the above equation has units of time. This quotient $\frac{x}{v}$ is basically the time spent by the medium in the tubular reactor at position x.[10] As such

$$\frac{x}{v} = t \tag{1.17}$$

yielding

$$c_x = c_0 \exp\left(-kt\right). \tag{1.18}$$

1.2.1 Non-dimensionalization

To get an intuitive understanding of the concentration profile, it is advantageous to cast the above expression into a so-called dimensionless form. This is done by renormalizing the units of concentration and time such that they are expressed relative to the inlet concentration and the total residence time in the reactor.[11] I define the dimensionless concentration as

[9] Alternatively, a plug-flow reactor is operated such that causality only propagates downstream and the conditions at a certain point in the reactor are not influenced by points further on in the reactor. By this simple reasoning, if we define the conditions at the very first point in the reactor, all the other conditions at further points downstream can be derived from that.

[10] If the medium would be carrying a clock and the clock would be set to zero at the inlet of the reactor, x/v would be the number of seconds displayed by that clock when the medium is at position x.

[11] This is basically what is meant by the word "renormalization". A new "norm" or unit is introduced to describe the properties.

$$\psi = \frac{c}{c_0} \tag{1.19}$$

and the mean residence time in the reactor τ by[12]

$$\tau = \frac{L}{v}. \tag{1.20}$$

Application of this coordinate transformation to Equation 1.16 yields

$$\psi = \exp\left(-k\tau\frac{x}{L}\right). \tag{1.21}$$

Observe now that the quotient $k\tau$ is a dimensionless number.[13] This dimensionless number is rather common within chemical reactor engineering and has been named after Gerhard Damköhler. The other quotient $\frac{x}{L}$ corresponds to the position in the reactor with respect to the total length of the reactor and is a dimensionless number as well. Introducing the variable λ to describe this latter quantity, we can rewrite Equation 1.21 as

$$\psi = \exp\left(-\mathrm{Da}\,\lambda\right). \tag{1.22}$$

Equation 1.22 is a fully dimensionless equation. All variables carry no dimensions and the domains of ψ and λ are both between 0 and 1. Although we have here defined λ as a dimensionless reactor coordinate, this variable is fully equivalent to a normalized time coordinate as given by

$$\lambda = \frac{x}{L} = \frac{t}{\tau}, \tag{1.23}$$

which can be readily confirmed by reviewing Equations 1.17 and 1.20. For the ideal plug-flow reactor, one can thus conclude that space and time are essentially the same variable linked via a coordinate transformation.[14]

Equation 1.22 is a highly abstracted form of a plug-flow reactor, but comes with a great advantage. This equation describes the concentration profile in **any** possible plug-flow reactor that meets the design criteria used to build this equation. In other words, whether you are looking at a 80m long tube or a 1cm long microreactor or whether you are looking at fast or slow kinetics, or fast or slow superficial velocities, you can calculate the characteristic variable Da and determine the concentration profile in the reactor by means of Equation 1.22.

Caution

Non-dimensionalization, although commonly employed in chemical reactor engineering, is not always possible for each system.

[12] This is the time the medium has spent, on average, in the reactor.

[13] Note that k has units of s^{-1} for a first-order reaction.

[14] Wherein the coordinate transformation can be constructed by means of the superficial velocity v and the length of the reactor L.

1.2.2 Direct derivation from microscopic balances

Instead of constructing the microscopic balance from first principles as we have done at the start of this chapter, it is quite common to take the general form of such a balance for a given coordinate system and adapt this balance to fit the system of interest. These microscopic balances are so ubiquitous in (chemical) engineering, that tables are made where one can directly take the microscopic balance from.[15] To exemplify upon the procedure, let us revisit the earlier problem of the tubular plug-flow reactor. A tubular reactor is best described using a cylindrical coordinate system. The microscopic balance for such a coordinate system is given by

[15] A good source would for example be the book "Transport Phenomena Data Companion" of Janssen and Warmoeskerken.[1]

$$\frac{\partial c}{\partial t} + \left(\frac{1}{r} \frac{\partial}{\partial r} \left(r N_r \right) + \frac{1}{r} \frac{\partial N_\theta}{\partial \theta} + \frac{\partial N_z}{\partial z} \right) = R, \tag{1.24}$$

wherein N_z is the molar flux defined in the coordinate direction z. For a plug-flow reactor, we assume that the concentration is independent of the radial r and angular θ directions. As such, the above equation can be simplified to yield

$$\frac{\partial c}{\partial t} + \left(\frac{1}{r} \cancel{\frac{\partial}{\partial r}} \left(r N_r \right) + \frac{1}{r} \cancel{\frac{\partial N_\theta}{\partial \theta}} + \frac{\partial N_z}{\partial z} \right) = R \tag{1.25}$$

$$\frac{\partial c}{\partial t} + \left(\frac{\partial N_z}{\partial z} \right) = R \tag{1.26}$$

which by introduction of Equation 1.11 and by noting that

$$\left(\frac{\partial N_z}{\partial z} \right) = v \frac{dc}{dz} \tag{1.27}$$

can be readily transformed to

$$\frac{\partial c}{\partial t} = -v \frac{\partial c}{\partial z} + R. \tag{1.28}$$

which is fully equivalent to the result of Equation 1.9.

The advantage of this procedure is that it can be readily generalized to systems of more complex geometry or when taking more dimensions into account. Furthermore, these microscopic balances not only exist for mass, but also for energy and motion.[16]

[16] Which corresponds to the Navier-Stokes equations.

1.3 Tanks-in-series approximation

The governing equation for a plug-flow reactor under the steady-state assumption yields the following ordinary differential equation

$$\frac{dc}{dx} = -\frac{kc}{v}. \tag{1.29}$$

If you look critical at the narrative of the preceding sections, we merely **claimed** that a solution exists and then postulated it. It is however

insightful to derive it from more basic principles. To do so, let us cut up the plug-flow reactor into equally sized cells for which we assume that these are sufficiently small so that the concentration can be considered to be uniform (i.e. independent of the position) within that cell. In other words, we describe the plug-flow reactor a series of continuously stirred tank reactors (CSTRs). A schematic depiction of this set-up is given in Figure 1.2.

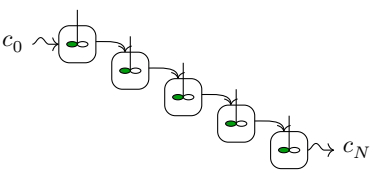

Figure 1.2: *Continuously-stirred tank reactors in series representation of the plug-flow reactor.*

These CSTRs have a very simple mole balance, which is given by the following **algebraic** expression[17]

$$(c_{i-1} - c_i) = kc_i t, \tag{1.30}$$

wherein c_i is the concentration within CSTR i. Observe now that c_{i-1} is the inlet concentration for CSTR i and corresponds to the outlet of CSTR $i-1$ and we can write a closed-form expression for the concentration in reactor i, which yields

$$c_i = \frac{c_{i-1}}{1+kt}. \tag{1.31}$$

Assume that we have N such tanks in series and that the inlet concentration of the first tank is given by c_0, then the concentration in the Nth tank is given by

$$C_N = c_0 \left(\frac{1}{1+kt/N}\right)^N, \tag{1.32}$$

wherein we have redefined t to be the **total** residence time through the whole series of CSTRs. Let us now explore the above equation into the limit when we cut up the PFR into an infinite number of CSTRs. This limit is given as

$$C_N = c_0 \lim_{N\to\infty} \left(\frac{1}{1+kt/N}\right)^N. \tag{1.33}$$

This turns out to be a converging series because each term in the series is much smaller than the previous term. It is actually relatively easy to determine this limit. By introduction of a natural logarithm, we can change the power in N to a multiplicative factor, as given by

[17] Assuming here a first-order reaction and steady-state.

$$C_N = c_0 \lim_{N\to\infty} \left(\frac{1}{1+kt/N}\right)^N \tag{1.34}$$

$$= c_0 \lim_{N\to\infty} \exp\left[\ln\left(\left(\frac{1}{1+kt/N}\right)^N\right)\right] \tag{1.35}$$

$$= c_0 \lim_{N\to\infty} \exp\left[N\ln\left(\frac{1}{1+kt/N}\right)\right] \tag{1.36}$$

$$= c_0 \lim_{N\to\infty} \exp\left[-N\ln\left(1+kt/N\right)\right] \tag{1.37}$$

$$= c_0 \exp\left[-\lim_{N\to\infty} N\ln\left(1+kt/N\right)\right] \tag{1.38}$$

$$= c_0 \exp\left[-\lim_{N\to\infty} \frac{\ln\left(1+kt/N\right)}{1/N}\right] \tag{1.39}$$

Although this form might look rather convoluted, it allows us to apply L'Hôpital's rule that states

$$\lim_{n\to\infty} \frac{f(n)}{g(n)} = \lim_{n\to\infty} \frac{f'(n)}{g'(n)} \tag{1.40}$$

by which we can solve for the limit, giving

$$C_N = c_0 \exp\left[-\lim_{N\to\infty} \frac{\ln\left(1+kt/N\right)}{1/N}\right] \tag{1.41}$$

$$= c_0 \exp\left[-\lim_{N\to\infty} \frac{\frac{\partial}{\partial N}\ln\left(1+kt/N\right)}{\frac{\partial}{\partial N}1/N}\right] \tag{1.42}$$

$$= c_0 \exp\left[-\lim_{N\to\infty} \frac{-\frac{kt}{N^2}\cdot\frac{1}{1+kt/N}}{-1/N^2}\right] \tag{1.43}$$

$$= c_0 \exp\left[-\lim_{N\to\infty} \frac{kt}{1+kt/N}\right] \tag{1.44}$$

$$= c_0 \exp\left[-kt\right] \tag{1.45}$$

This result is identical to the solution seen earlier in Equation 1.18. Interestingly, this simple example convinces us that it is possible to cast an ordinary differential equation into a set of algebraic equations which in the limit of $N \to \infty$, yields the exact result. Perhaps more importantly, the reason that the limit is finite is because the series expansion rapidly converges. As such, it is likely to assume that with even a modest amount of cells N, we obtain a very good approximation of the exact solution. As such, it is interesting to see if we can generalize this procedure to other systems.

1.4 Exercises

Exercise 1.1

a) Consider the approximation of the concentration profile in a plug-flow reactor (PFR) by using a tanks-in-series approach. Determine the root-mean-squared-error (RMSE) as given by

$$\mathrm{RMSE} = \sqrt{\frac{\sum_{i=1}^{N}(x_i - \hat{x}_i)^2}{N}}, \tag{1.46}$$

where $\{x_i\}$ are the predicted points and $\{\hat{x}_i\}$ the points according to the analytical (exact) solution. Take the following conditions

- Work in non-dimensionalized coordinates.
- Use $\mathrm{Da} = 3$.
- Assume the tanks are equivalent in volume and distributed uniformly.

Show that when using $N = 10$ tanks, that the RMSE corresponds to (approximately) `0.0386`. Create a graph wherein you plot the concentration per tank versus the analytical solution

$$\psi = \exp(-\mathrm{Da} \cdot \lambda), \tag{1.47}$$

where $\psi, \lambda \in (0, 1)$ correspond to the non-dimensionalized concentration and axial position, respectively.

Note that the "position" of the first tank corresponds to $\lambda = 1/N$ and **not** to $\lambda = 0$.

b) Determine the minimum number of tanks required to achieve a RMSE less than 10^{-4}. Perform a linear fit in double-log space by means of

$$\ln(\mathrm{RMSE}) = a \ln(N) + b \tag{1.48}$$

such that once you have established values for a and b, you can determine N_{min} via

$$N = \exp\left(\frac{\ln(\mathrm{RMSE}) - b}{a}\right). \tag{1.49}$$

.

2 FINITE DISCRETIZATION METHODS

Contents

2.1 Introduction

In the previous chapter, we demonstrated that through discretization, an ordinary differential equation can be transformed into a system of coupled algebraic equations. In this chapter, we build upon that foundation by introducing two discretization techniques widely used in chemical reactor engineering: the finite difference method and the finite volume method.[1]

For most students, the finite difference method is the first discretization approach encountered. From a pedagogical standpoint, we begin with a concise review of its fundamental principles. We then introduce the finite volume method, which will serve as the primary numerical framework for the remainder of this text. Finally, we discuss how to evaluate the accuracy of a numerical method — whether finite difference or finite volume — and examine how the associated error scales with the resolution of the discretization grid.

[1] A third approach, the finite element method, also exists. Although more complex and therefore beyond the scope of this book, it offers significant advantages when dealing with systems of irregular or complex geometry.

2.2 Finite difference method

A straightforward way to numerically approximate the concentration profile in a plug-flow reactor is through the finite difference method. In this method, a set of discrete points[2] is defined along the reactor length, and algebraic relationships between these points are established. The governing equation for steady-state operation with a first-order reaction is given by

[2] Typically distributed on an equidistant grid.

$$\frac{dc}{dx} = -\frac{kc}{v}. \tag{2.1}$$

In dimensionless form, this equation can be written as

$$\frac{d\psi}{d\lambda} = -\,\mathrm{Da}\,\psi, \tag{2.2}$$

where λ denotes the dimensionless reactor length (ranging from 0 to 1), ψ the dimensionless concentration (also between 0 and 1), and Da the dimensionless Damköhler number, as introduced earlier.

This equation applies to all points *within* the reactor domain. To solve this first-order differential equation, one boundary condition must be specified. Here, the concentration at the reactor inlet is known, corresponding to a Dirichlet boundary condition:

$$\psi|_{\lambda=0} = 1. \tag{2.3}$$

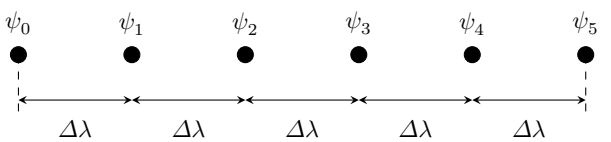

Figure 2.1: *Schematic depiction of the (equidistant) grid used in the finite difference approximation of the plug-flow reactor. The dashed lines indicate the domain boundaries.*

Consider now the equidistant grid shown schematically in Figure 2.1. Two grid points coincide with the reactor boundaries, representing the inlet and outlet. This grid distribution is not unique, and alternative arrangements may be used.[3] For all internal points ψ_i with $i \neq 0$, Equation 2.2 is valid. The boundary point satisfies $\psi_0 = 1$.

The derivative at each interior point ψ_i $\forall i \notin (0, N-1)$ can be approximated[4] using the central difference formula[5]:

$$\frac{\partial \psi_i}{\partial \lambda} \approx \frac{\psi_{i+1} - \psi_{i-1}}{2\Delta\lambda}. \tag{2.4}$$

For the boundary points, we apply

$$\psi_0 = 1, \tag{2.5}$$

$$\psi_{N-1} \approx \frac{\psi_{N-1} - \psi_{N-2}}{\Delta\lambda}, \tag{2.6}$$

where

$$\Delta\lambda = \frac{1}{N-1}. \tag{2.7}$$

Substituting Equation 2.4 into Equation 2.2 yields the following set of linear equations:

[3] It is ultimately up to the engineer to select the grid distribution that best suits the problem at hand.

[4] If you are unfamiliar with this approximation, consider it as given for now. Its derivation is discussed later in Section 2.4.

[5] This is not the only possible choice. In fact, for plug-flow systems without back-mixing, an upwind (backward) difference scheme would be more physically appropriate which we will demonstrate at the end of this section.

$$1 = \psi_0, \tag{2.8}$$

$$0 = \frac{\psi_{i+1} - \psi_{i-1}}{2\Delta\lambda} + \mathrm{Da}\,\psi_i, \quad \forall i \notin (0, N-1), \tag{2.9}$$

$$0 = \frac{\psi_{N-1} - \psi_{N-2}}{\Delta\lambda} + \mathrm{Da}\,\psi_{N-1}. \tag{2.10}$$

This system can be expressed in matrix–vector form as

$$\mathbf{A}\vec{\psi} = \vec{b}, \tag{2.11}$$

where the matrix $\mathbf{A}$ is defined as

$$\mathbf{A} = \begin{pmatrix} 1 & 0 & 0 & 0 & \cdots & 0 & 0 & 0 & 0 \\ -1 & 2\,\mathrm{Da}\,\Delta\lambda & 1 & 0 & \cdots & 0 & 0 & 0 & 0 \\ 0 & -1 & 2\,\mathrm{Da}\,\Delta\lambda & 1 & \cdots & 0 & 0 & 0 & 0 \\ \vdots & & & & \ddots & & & & \vdots \\ 0 & 0 & 0 & 0 & \cdots & -1 & 2\,\mathrm{Da}\,\Delta\lambda & 1 & 0 \\ 0 & 0 & 0 & 0 & \cdots & 0 & -1 & 2\,\mathrm{Da}\,\Delta\lambda & 1 \\ 0 & 0 & 0 & 0 & \cdots & 0 & 0 & -1 & 1 + \mathrm{Da}\,\Delta\lambda \end{pmatrix}, \tag{2.12}$$

and the corresponding right-hand side vector is

$$\vec{b} = \begin{pmatrix} 1 \\ 0 \\ \vdots \\ 0 \end{pmatrix}. \tag{2.13}$$

For the case of $N = 6$ grid points, the resulting 6×6 system becomes

$$\mathbf{A} = \begin{pmatrix} 1 & 0 & 0 & 0 & 0 & 0 \\ -1 & 2\,\mathrm{Da}\,\Delta\lambda & 1 & 0 & 0 & 0 \\ 0 & -1 & 2\,\mathrm{Da}\,\Delta\lambda & 1 & 0 & 0 \\ 0 & 0 & -1 & 2\,\mathrm{Da}\,\Delta\lambda & 1 & 0 \\ 0 & 0 & 0 & -1 & 2\,\mathrm{Da}\,\Delta\lambda & 1 \\ 0 & 0 & 0 & 0 & -1 & 1 + \mathrm{Da}\,\Delta\lambda \end{pmatrix}, \tag{2.14}$$

and

$$\vec{b} = \begin{pmatrix} 1 \\ 0 \\ 0 \\ 0 \\ 0 \\ 0 \end{pmatrix}. \tag{2.15}$$

The solution to Equation 2.11 can be obtained using any linear solver. The results for $N = 6$ grid points are shown in Figure 2.2. The dashed

line corresponds to the analytical solution given by Equation 1.22. The numerical and analytical solutions show good agreement, and the accuracy can be improved by increasing the number of grid points.

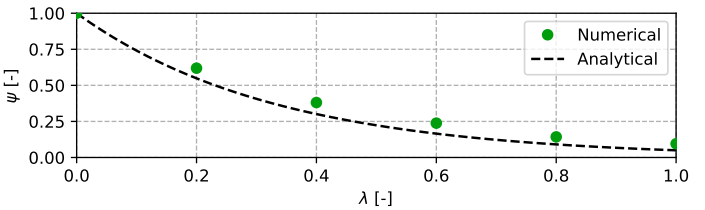

Figure 2.2: *Dimensionless concentration profile of a plug-flow reactor as a function of the dimensionless length for* $\mathrm{Da} = 3$ *using* $N = 6$ *equidistant grid points. The first and last grid points coincide with the domain boundaries.*

As noted earlier, the positioning of the grid points is not unique, and alternative discretization strategies can improve accuracy. Instead of placing the first and last grid points exactly at the boundaries, they are shifted inward by half a grid spacing. To maintain consistency, six grid points are still used. A schematic representation of this arrangement is shown in Figure 2.3.

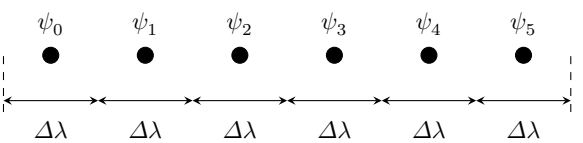

Figure 2.3: *Schematic depiction of the equidistant grid used in the finite difference approximation of the plug-flow reactor. The grid points are shifted inward by half a grid spacing from the domain boundaries, which are indicated by the dashed lines.*

In this offset scheme, the first derivative can be approximated using a backward difference scheme:

$$\frac{\partial \psi_i}{\partial \lambda} \approx \frac{\psi_i - \psi_{i-1}}{\Delta\lambda}, \quad \forall i \neq 0. \tag{2.16}$$

At the inlet, the Dirichlet boundary condition is incorporated via

$$\frac{\partial \psi_0}{\partial \lambda} \approx \frac{1 - \psi_0}{\Delta\lambda/2}. \tag{2.17}$$

Implementation of these approximations into Equation 2.2 yields the following matrix representation:

$$\mathbf{A} = \begin{pmatrix} 1+\mathrm{Da}\,\Delta\lambda/2 & 0 & 0 & 0 & 0 & 0 \\ -1 & 1+\mathrm{Da}\,\Delta\lambda & 0 & 0 & 0 & 0 \\ 0 & -1 & 1+\mathrm{Da}\,\Delta\lambda & 0 & 0 & 0 \\ 0 & 0 & -1 & 1+\mathrm{Da}\,\Delta\lambda & 0 & 0 \\ 0 & 0 & 0 & -1 & 1+\mathrm{Da}\,\Delta\lambda & 0 \\ 0 & 0 & 0 & 0 & -1 & 1+\mathrm{Da}\,\Delta\lambda \end{pmatrix}, \tag{2.18}$$

and

$$\vec{b} = \begin{pmatrix} 1 \\ 0 \\ 0 \\ 0 \\ 0 \\ 0 \end{pmatrix}. \tag{2.19}$$

The solution of this system, along with a comparison to the analytical solution, is shown in Figure 2.4.

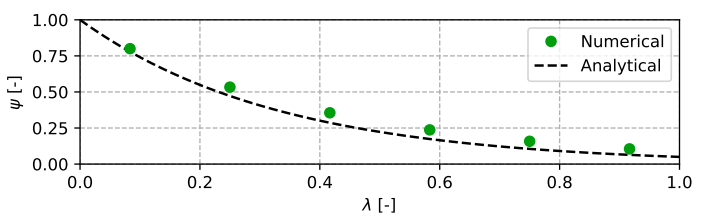

Figure 2.4: *Dimensionless concentration profile of a plug-flow reactor as a function of the dimensionless length for* $\mathrm{Da} = 3$ *using* $N = 6$ *equidistant grid points. The first and last grid points are positioned half a grid spacing inside the domain boundaries.*

Using two different numerical approximation strategies allows for a direct quantitative comparison. A convenient way to measure their relative accuracy is via the mean absolute error (MAE), defined as

$$\mathrm{MAE} = \frac{1}{N}\sum_{i=1}^{N} |x_i - \hat{x}_i|\,, \tag{2.20}$$

where x_i are the numerical results and $\hat{x}_i$ the analytical values.

For the first discretization scheme, the MAE is 0.0534, while for the second it decreases slightly to 0.0514. Although the difference is small, this confirms that the modified grid and derivative approximation provide a marginally more accurate result. In Section 2.4, we will show how to *devise* discretization equations for derivatives of any order, enabling higher-order approximations. Subsequently, in Section 2.5, we will discuss how to evaluate the accuracy of numerical schemes and how the error

scales with the grid resolution. Before that, however, we first introduce the finite volume method in the next section.

2.3 Finite volume method

If we consider the Tanks-in-Series approximation of the tubular plug-flow reactor as shown in Chapter 1, the infinitesimal description of the problem (i.e., the microbalance or ordinary differential equation) is effectively transformed into a series of finite, well-defined cells. This concept lies at the heart of the *finite volume method*.

In essence, the finite volume method enforces conservation laws over discrete, finite regions of space rather than at infinitesimal points. Given a microbalance and a set of boundary and/or initial conditions, the spatial domain is subdivided into a number of control volumes, for which algebraic balance equations are formulated. The dependent variables in these equations are, in part, shared between neighboring control volume. In other words, similar to the finite difference method, the resulting algebraic equations are **linked**.

To introduce the method, let us again revisit the plug-flow reactor problem. Assuming steady-state conditions and a first-order reaction, the governing differential equation is given by Equation 2.2, and its boundary condition by Equation 2.3. To construct the finite volume formulation, we discretize the domain into N equally sized control volumes of dimensionless length $1/N$. A schematic depiction of this discretization is shown in Figure 2.5.

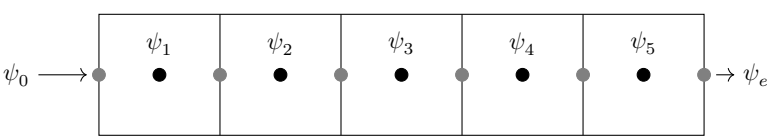

Figure 2.5: *Schematic depiction of the discretization of the tubular reactor using 5 control volumes. For each control volume, only the concentration at the center of the control volume is known, as indicated by the black circles, and assumed to be uniform over the whole control volume. The values at the boundaries, indicated by gray circles, are undefined and need to be obtained using interpolation techniques. For the concentration at the west edge for the first control volume, the concentration is set by the boundary condition and corresponds to the inlet concentration ψ_0.*

We furthermore assume that the concentration ψ is uniform **fully within** each control volume.[6] Rather than writing the differential equation directly, we now express the conservation of ψ over a finite region of space. In the most general form, this conservation statement reads

$$\int_V \nabla \cdot \vec{F}\, dV = -\int_V \mathrm{Da}\, \psi\, dV, \tag{2.21}$$

[6] This means that the concentration ψ at the boundaries of the control volumes needs to be interpolated.

where $\vec{F}$ denotes the flux of ψ across the control volume boundaries. This equation expresses that the net flux through the surface enclosing a control volume equals the total rate of reaction (or consumption) within that volume. It forms the fundamental basis of the finite volume method.

For the one-dimensional plug-flow reactor, the flux $\vec{F}$ reduces to convective transport along the axial coordinate λ, and Equation 2.21 simplifies to

$$A_\perp \int_{\lambda_w}^{\lambda_e} \frac{d\psi}{d\lambda}\, d\lambda = -A_\perp \,\mathrm{Da} \int_{\lambda_w}^{\lambda_e} \psi\, d\lambda, \tag{2.22}$$

where $A_\perp$ represents the reactor's cross-sectional area. Because $A_\perp$ is constant, the infinitesimal volume element can be written as $dV = A_\perp\, d\lambda$, giving

$$\int_V \frac{d\psi}{d\lambda}\, dV = -\int_V \mathrm{Da}\, \psi\, dV. \tag{2.23}$$

Although expressed here for a one-dimensional system, Equation 2.23 directly generalizes to higher dimensions by replacing the spatial derivative $\frac{d\psi}{d\lambda}$ with the divergence operator $\nabla \cdot \vec{F}$, where V then represents an arbitrary control volume in space.

Since the integral in Equation 2.23 is taken over a closed and well-defined control volume, we can apply the divergence theorem to convert the volume integral of the divergence into a surface integral of the flux across the boundaries:[7]

$$\iiint_V \left(\nabla \cdot \vec{F}\right) dV = \oiint_S \left(\vec{F} \cdot \hat{n}\right) dS, \tag{2.24}$$

where S denotes the surface enclosing the control volume, $\vec{F}$ is the flux vector, and $\hat{n}$ is the outward-pointing unit normal vector. This transformation converts the differential (pointwise) conservation equation into an integral (flux-based) form, which forms the mathematical foundation of the finite volume method.

[7] In general, the finite volume method always applies to closed regions, which allows the divergence theorem (or its one-dimensional analogue) to be used.

For a purely one-dimensional problem, this expression simplifies to

$$\int_a^b \frac{df(x)}{dx}\, dx = f(b) - f(a), \tag{2.25}$$

which corresponds to the well-known fundamental theorem of calculus.[2]

$$A \int_{\lambda_w}^{\lambda_e} \frac{d\psi}{d\lambda}\, d\lambda = A\left[\psi(\lambda_e) - \psi(\lambda_w)\right], \tag{2.26}$$

which, after adding the right-hand side of Equation 2.23, yields

$$A_\perp \psi_e - A_\perp \psi_w = -\,\mathrm{Da}\, \psi_P \Delta V. \tag{2.27}$$

Here, the subscripts P, w, and e refer to the central control volume and the nodes at its west and east boundaries, respectively. A schematic

of this notation is shown in Figure 2.6. The centers of the neighboring west and east control volumes are denoted by W and E. Dividing both sides of Equation 2.27 by $A_\perp$ gives

$$\psi_e - \psi_w = -\,\mathrm{Da}\,\Delta\lambda\,\psi_P, \tag{2.28}$$

where $\Delta\lambda = 1/N$ is the length of a single control volume.

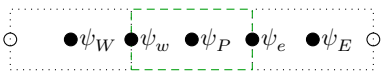

Figure 2.6: *Notation for control volume P and its neighboring nodes. Capital letters denote cell centers (W, P, E), while lowercase letters indicate the corresponding boundary faces (w, e).*

Because the concentration is known only at the cell centers (the ψ_P values) and not at the boundaries (ψ_w and ψ_e), the boundary concentrations must be approximated.[8] A common approach is to use linear interpolation, corresponding to the arithmetic mean of the two adjacent cell-center values:[9]

$$\psi_e = \frac{\psi_E + \psi_P}{2}, \tag{2.29}$$

$$\psi_w = \frac{\psi_W + \psi_P}{2}. \tag{2.30}$$

Substituting these expressions gives

$$\frac{\psi_E + \psi_P}{2} - \frac{\psi_W + \psi_P}{2} = -\,\mathrm{Da}\,\Delta\lambda\,\psi_P, \tag{2.31}$$

which simplifies to

$$\left(-\frac{1}{2}\right)\psi_W + (\mathrm{Da}\,\Delta\lambda)\,\psi_P + \left(\frac{1}{2}\right)\psi_E = 0. \tag{2.32}$$

For each control volume, an equation of the form Equation 2.32 is obtained, except at the boundaries. For the first and last cells, modified formulations are required since there are no neighboring cells on one side.

For the first cell, the west face concentration is prescribed by the boundary condition:

$$\psi_w = \psi_0. \tag{2.33}$$

For the last cell, the east face concentration is assumed equal to that at the cell center:

$$\psi_e = \psi_P. \tag{2.34}$$

These yield the following equations for the first and last control volumes:

$$\left(\frac{1}{2} + \mathrm{Da}\,\Delta\lambda\right)\psi_P + \left(\frac{1}{2}\right)\psi_E = \psi_0, \tag{2.35}$$

$$\left(-\frac{1}{2}\right)\psi_W + \left(\frac{1}{2} + \mathrm{Da}\,\Delta\lambda\right)\psi_P = 0. \tag{2.36}$$

It is convenient to express all these equations in a standardized form:

$$\boxed{a_W\psi_W + a_P\psi_P + a_E\psi_E = b,} \tag{2.37}$$

[8] Each boundary is shared by two neighboring cells; hence, it cannot simultaneously take on distinct values for both.

[9] Since the cells are of equal size, the midpoint value corresponds to a simple average.

[10] For instance, terms arising from boundary conditions.

where a_W, a_P, and a_E are coefficients associated with the control volume and its neighbors, and b represents source or boundary terms.[10] Using this notation, the finite volume coefficients can be summarized as shown in Table 2.1.

Table 2.1: *Finite volume discretization coefficients for the tubular plug-flow reactor.*

Terms	a_W	a_P	a_E	b
$i = 0$	0	$\frac{1}{2} + \mathrm{Da}\,\Delta\lambda$	$\frac{1}{2}$	$\psi(0)$
$0 < i < N-1$	$-\frac{1}{2}$	$\mathrm{Da}\,\Delta\lambda$	$\frac{1}{2}$	0
$i = N-1$	$-\frac{1}{2}$	$\frac{1}{2} + \mathrm{Da}\,\Delta\lambda$	0	0

In Equations 2.32, 2.35 and 2.36, ψ_E and ψ_W correspond to concentrations in adjacent cells. Hence, the system consists of coupled linear equations that can be expressed compactly in matrix form as

$$\mathbf{A}\vec{\psi} = \vec{b}. \tag{2.38}$$

For $N = 5$ control volumes, the coefficient matrix $\mathbf{A}$ and source vector $\vec{b}$ are

$$\mathbf{A} = \begin{pmatrix} \frac{1}{2} + \mathrm{Da}\,\Delta\lambda & \frac{1}{2} & 0 & 0 & 0 \\ -\frac{1}{2} & \mathrm{Da}\,\Delta\lambda & \frac{1}{2} & 0 & 0 \\ 0 & -\frac{1}{2} & \mathrm{Da}\,\Delta\lambda & \frac{1}{2} & 0 \\ 0 & 0 & -\frac{1}{2} & \mathrm{Da}\,\Delta\lambda & \frac{1}{2} \\ 0 & 0 & 0 & -\frac{1}{2} & \frac{1}{2} + \mathrm{Da}\,\Delta\lambda \end{pmatrix}, \tag{2.39}$$

$$\vec{b} = \begin{pmatrix} \psi_0 \\ 0 \\ 0 \\ 0 \\ 0 \end{pmatrix}. \tag{2.40}$$

Solving this linear system[11] yields the dimensionless concentration profile shown in Figure 2.7. The numerical solution obtained with the finite volume method is in excellent agreement with the analytical solution.

[11] Here using $\mathrm{Da} = 3$.

2.4 Finite difference coefficients

Regardless of whether one uses the finite difference or the finite volume method, both approaches ultimately rely on approximating spatial derivatives by means of linear combinations of function values at discrete points. The coefficients of these linear combinations, known as *finite difference coefficients*, determine the accuracy of the approximation. In what follows,

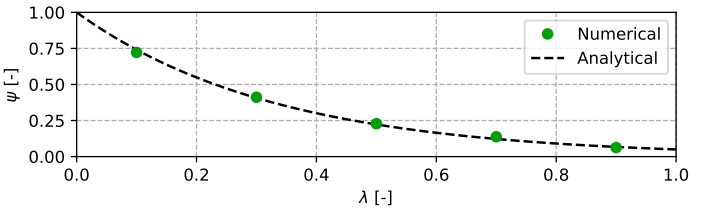

Figure 2.7: *Dimensionless concentration profile of a plug-flow reactor as a function of the dimensionless length for* $\mathrm{Da} = 3$. *The symbols indicate the finite volume solution, and the dashed line represents the analytical result.*

we develop a general framework for determining these coefficients from first principles.

Suppose we have a point in space x_0 whose n^{th}-order derivative we wish to approximate by means of a sum of linear coefficients as given by

$$\frac{\partial^n f}{\partial x^n}(x_0) \approx \sum_i c_i f(x_i). \tag{2.41}$$

For the point of interest at x_0, a Taylor series with respect to the adjacent points $x_i \forall i \neq 0$ can be constructed as given by

$$f(x_i) = \sum_{n=0}^{\infty} \frac{\partial^{(n)} f(x_0)}{\partial x^{(n)}} \frac{(x_i - x_0)^n}{n!} \tag{2.42}$$

$$= f(x_0) + \frac{\partial f(x_0)}{\partial x} \frac{(x_i - x_0)}{1} + \frac{\partial^2 f(x_0)}{\partial x^2} \frac{(x_i - x_0)^2}{2} + \frac{\partial^3 f(x_0)}{\partial x^3} \frac{(x_i - x_0)^3}{6} + \dots \tag{2.43}$$

For each point x_i, we thus have one such Taylor series and all these individual Taylor series share terms $\frac{\partial^n f}{\partial x^n}(x_0)$. One of these terms corresponds to the derivative at the point of interest whose value we aim to approximate. To work towards this aim, let us multiply all Taylor series as shown in Equation 2.43 by a (yet) unknown constant c_i and add all these series together. We then find

$$\sum_i c_i f(x_i) = \sum_i \left(\sum_{n=0}^{\infty} \frac{c_i \, (x_i - x_0)^n}{n!} \frac{\partial^n f}{\partial x^n} \, (x_0) \right) = \frac{\partial^k f}{\partial x^k} \, (x_0) \,, \tag{2.44}$$

where we have set this sum equal to the k^{th} order derivative we aim to approximate.[12] Equation 2.44 expands into N individual equations, with N corresponding simultaneously to the number of sampling points employed in the discretization and to the highest order retained in the truncated Taylor expansion.[13] The resulting system of equations is given by

[12] The derivative we aim to approximate corresponds to the last term in Equation 2.44.

[13] From this connection, one can directly observe that using more sampling points leads to a higher-order Taylor approximation and therefore a more accurate estimate of the derivative.

$$\left\{ \sum_i \frac{c_i \left(x_i - x_0\right)^n}{n!} \frac{\partial^n f}{\partial x^n}\left(x_0\right) = \delta_{nk} \frac{\partial^k f}{\partial x^k}\left(x_0\right) \right\}, \tag{2.45}$$

wherein we have used the Kronecker delta to indicate that for only one of these equations the right-hand side is non-zero, corresponding to the derivative we aim to approximate. If set the number of equations N equal to the number of points we use to approximate the derivative, then Equation 2.45 essentially represents a system of N equations with N unknowns. Such systems can be represented as a matrix-vector equation as given by

$$\mathbf{T}\vec{c} = \vec{b}, \tag{2.46}$$

wherein the terms T_{ni} in the matrix $\mathbf{T}$ are given by

$$T_{ni} = \left(x_i - x_0\right)^n \tag{2.47}$$

and which upon multiplication by a vector $\vec{c} = (\cdots, c_{-2}, c_{-1}, c_0, c_1, c_2, \cdots)$ would yield a vector $\vec{b}$ where[14]

$$b_k = \delta_{ik} \cdot k! \tag{2.48}$$

In other words, the only element in $\vec{b}$ that has a non-zero value is that element whose index matches the derivative we set out to approximate. Once the matrix $\mathbf{T}$ and the solution vector $\vec{b}$ are constructed, a linear solver[15] can be readily used to find the values for the coefficient vector $\vec{c}$.

The generalized mathematical procedure as shown above is probably a bit daunting to comprehend and therefore allow me to simplify it using a number of examples. Suppose we aim to construct a finite difference approximation for a first-order derivative at a point using the value at the point itself and its two neighbors, as shown schematically in Figure 2.8. For simplicity, we assume that adjacent points are equidistant by a distance h.

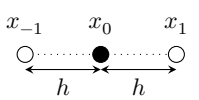

Figure 2.8: *Schematic depiction of a three point stencil where the first-order derivative is approximated at the central point.*

In this example, the matrix $\mathbf{T}$ would host the following values[16]

$$\mathbf{T} = \begin{pmatrix} 1 & 1 & 1 \\ -h & 0 & h \\ h^2 & 0 & h^2 \end{pmatrix} \tag{2.49}$$

and for the solution vector $\vec{b}$ the values

$$\mathbf{b} = \begin{pmatrix} 0 \\ 1 \\ 0 \end{pmatrix}. \tag{2.50}$$

One could fill out the numerical value for h in the above equation and solve it, yet if we solve the system **in terms of** h, we can produce a

[14] Observe that I have migrated the common term $n!$ from the left hand side in Equation 2.45 to the right.

[15] If you are using Python, one would use "numpy.linalg.solve".

[16] For a proper understanding of the procedure, the reader is kindly invited to try to reproduce these values.

somewhat more generalized solution valid for any chosen regular lattice. To do so, we note that for every linear equation that equals zero, we can remove the terms in h^n by division.[17] For the remaining equation that has a non-zero result, the h^n term is migrated to the right hand side by which the coefficients c_i are expressed in units of $1/h^i$.

[17] The seminal work of the Indian mathematician Brahmagupta teaches us that 0 divided by a finite value yields 0.

Application of this strategy to the above two equations, yields

$$\mathbf{T} = \begin{pmatrix} 1 & 1 & 1 \\ -1 & 0 & 1 \\ 1 & 0 & 1 \end{pmatrix} \tag{2.51}$$

and for the solution vector $\vec{b}$ the values

$$\vec{b} = \begin{pmatrix} 0 \\ 1 \\ 0 \end{pmatrix}. \tag{2.52}$$

[18] Note that this vector is expressed in units of $\frac{1}{h}$.

It can be easily seen that vector $\vec{c}$ which solves Equation 2.46 corresponds to[18]

$$\vec{c} = \begin{pmatrix} -1/2 \\ 0 \\ 1/2 \end{pmatrix}. \tag{2.53}$$

Since the coefficient vector $\vec{c}$ was defined in units of $\frac{1}{h}$, reintroducing this scaling factor yields the final finite difference discretization

$$\frac{\partial f}{\partial x} \approx \frac{f(x_1) - f(x_{-1})}{2h}. \tag{2.54}$$

I hope this solution is extremely familiar to you as it is similar to how we would approximate the slope $s \approx \delta y / \delta x$.

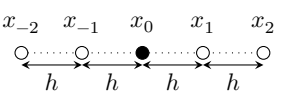

Figure 2.9: *Schematic depiction of a five point stencil where the second-order derivative is approximated at the central point.*

Repetition is the mother of learning[19], so let us look into another example. Suppose we wish to approximate the **second**-order derivative for a central point surrounded by two points on each side, as shown schematically in Figure 2.9. All points are equidistant with respect to their neighbors. Under these conditions, the matrix $\mathbf{T}$ would be[20]

$$\mathbf{T} = \begin{pmatrix} 1 & 1 & 1 & 1 & 1 \\ -2 & -1 & 0 & 1 & 2 \\ 4 & 1 & 0 & 1 & 4 \\ -8 & -1 & 0 & 1 & 8 \\ 16 & 1 & 0 & 1 & 16 \end{pmatrix}. \tag{2.55}$$

and the corresponding solution vector $\vec{b}$ is given by[21]

[19] ...and mistakes are the best teacher

[20] Here, I have skipped on the step of first constructing a matrix with all the h^n terms and immediately write down the numerical result.

[21] Note that the 2 in this equation arises from the 2!.

$$\vec{b} = \begin{pmatrix} 0 \\ 0 \\ 2 \\ 0 \\ 0 \end{pmatrix}. \tag{2.56}$$

Solving Equation 2.46 for this system yields the following coefficient vector[22]

[22] Recall that this vector is expressed in units of $\frac{1}{h^2}$.

$$\vec{c} = \begin{pmatrix} -1/12 \\ 4/3 \\ -5/2 \\ 4/3 \\ -1/12 \end{pmatrix}. \tag{2.57}$$

by which we find the following approximation for the second-order derivative[23]

[23] To clean up this equation, I have expressed everything using a common denominator.

$$\frac{\partial^2 f}{\partial x^2} \approx \frac{-1f(x_{-2}) + 16f(x_{-1}) - 30f(x_0) + 16f(x_1) - 1f(x_2)}{12h^2}. \tag{2.58}$$

Online resource

For **equidistant** grids, the most commonly used type of grid in finite difference approximations, one can use an online finite difference calculator to establish the coefficients. See: https://finite-difference-coefficients.nl/.

The procedure described above is not restricted to equidistant grids, nor to cases where the point of interest is surrounded by neighboring points. To illustrate this, consider approximating the first-order derivative at a boundary point using the point itself and two additional points located to its right. The first neighboring point is positioned at a distance of $\frac{h}{2}$, and the second at $\frac{3h}{2}$. The configuration is schematically depicted in Figure 2.10. We would find the following matrix $\mathbf{T}$

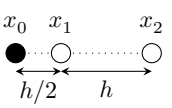

Figure 2.10: *Schematic depiction of a three point stencil where the first-order derivative is approximated for the most left point.*

$$\mathbf{T} = \begin{pmatrix} 1 & 1 & 1 \\ 0 & 1/2 & 3/2 \\ 0 & 1/4 & 9/4 \end{pmatrix} \tag{2.59}$$

and for the solution vector $\vec{b}$ the values

$$\vec{b} = \begin{pmatrix} 0 \\ 1 \\ 0 \end{pmatrix}. \tag{2.60}$$

[24] Note that $\vec{c}$ is expressed in units of $\frac{1}{h}$.

The vector $\vec{c}$ which solves Equation 2.46 yields[24]

$$\vec{c} = \begin{pmatrix} -8/3 \\ 3 \\ -1/3 \end{pmatrix}. \tag{2.61}$$

giving the following finite difference approximation

$$\frac{\partial f}{\partial x} \approx \frac{-8f(x_0) + 9f(x_1) - 1f(x_2)}{3h}. \tag{2.62}$$

Remember

From the above examples, observe that to approximate the k^{th} derivative, we need at least $k+1$ sampling points.

2.5 Error analysis and the order of a method

Numerical models are inherently approximations of the (idealized) physical systems they represent. To assess the accuracy of a numerical model, it must be compared against the exact analytical solution[25]. Several metrics are commonly used to quantify the accuracy of a numerical procedure. Among the most widely applied are the root-mean-squared error (RMSE), the mean absolute error (MAE), and the mean absolute percentage error (MAPE). These metrics share a key property: they all describe the *average* error per data point. This normalization is important, as the total error should not increase merely because more data points are used. In fact, a well-behaved numerical method should show a decrease in the mean error as the number of grid points increases. The RMSE, MAE, and MAPE are defined as follows:

[25] At least, when such an exact solution exists.

$$\text{RMSE} = \frac{1}{N}\sqrt{\sum_{i=1}^{N}(x_i - \hat{x}_i)^2}, \tag{2.63}$$

$$\text{MAE} = \frac{1}{N}\sum_{i=1}^{N}|x_i - \hat{x}_i|, \tag{2.64}$$

$$\text{MAPE} = \frac{1}{N}\sum_{i=1}^{N}\frac{|x_i - \hat{x}_i|}{\hat{x}_i}, \tag{2.65}$$

where x_i denotes the model prediction, $\hat{x}_i$ the exact value, and N the total number of data points.

A particularly important characteristic of a numerical method is how its accuracy scales with the (spatial) step size $\Delta\lambda$. This property is referred to as the **order of the method**, and it can be empirically determined using

$$\mathcal{O} = \frac{\partial \ln(E)}{\partial \ln(\Delta\lambda)}, \tag{2.66}$$

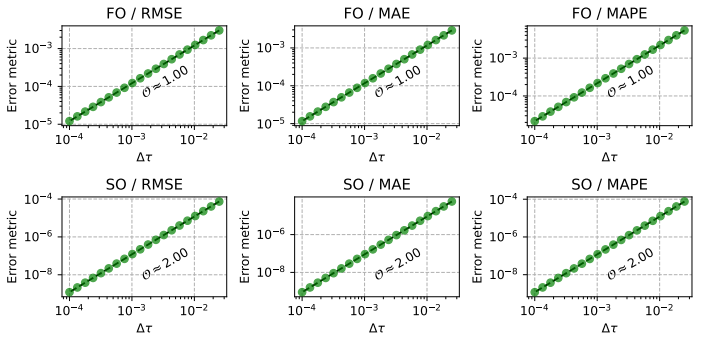

Figure 2.11: *Mean error as a function of the step size $\Delta\lambda$. The dashed black lines represent linear fits to the data. The slope of each fit corresponds to the order of the method, $\mathcal{O}$. "FO" and "SO" refer to first- and second-order methods, respectively.*

where E is the chosen error metric. For a first-order method ($\mathcal{O} = 1$), halving the step size (or equivalently doubling the number of grid points) reduces the mean error by a factor of two. For a second-order method ($\mathcal{O} = 2$), the error decreases by a factor of four, and for a third-order method ($\mathcal{O} = 3$), reducing the step size by a factor of ten would reduce the error by roughly a factor of 1000. Clearly, the order of a method is a key indicator of its efficiency in achieving a desired accuracy.

A practical way to determine $\mathcal{O}$ is to plot an error metric (e.g., RMSE, MAE, or MAPE) against the step size $\Delta\lambda$ on a double-logarithmic plot and fit a straight line through the data points. The slope of this line corresponds to the order of the method, as illustrated in the top three panels of Figure 2.11. From these plots, we find that the discretization procedure introduced in Section 2.3 exhibits a slope of $\mathcal{O} = 1$, confirming that it is a first-order method.

The order of a method is closely tied to the number of data points used to approximate a derivative. In the example from Section 2.3, effectively two data points (ψ_E and ψ_W) are used to approximate a first-order derivative, yielding a first-order accurate scheme. To improve the order of accuracy, additional points must be included in the discretization stencil.

As an illustration, let us construct a numerical scheme with second-order accuracy, where the mean error decreases quadratically with the step size. Instead of using two data points to approximate the derivative, we now employ three. Moreover, because the concentration profile in a plug-flow reactor depends only on upstream conditions, we use a so-called **upwind** discretization scheme, in which only points preceding the point of interest are included in the derivative approximation.[26] For any point beyond the second grid point, this leads to the following discretization:

$$\frac{\psi_{WW} - 4\psi_W + \psi_P}{2\Delta\lambda} = \mathrm{Da}\,\psi_P, \tag{2.67}$$

[26] The detailed derivation of this upwind scheme is not critical for the present discussion. It is provided here mainly to enable reproduction of the results, should the reader wish to do so.

where ψ_{WW} refers to the second control volume to the left of ψ_P. For the first and second grid points, the boundary conditions yield the following relations:

$$\frac{\psi_0 - \psi_P}{\Delta\lambda/2} = \mathrm{Da}\,\psi_P, \tag{2.68}$$

and

$$\frac{4\psi_0 - 9\psi_W + 5\psi_P}{3\Delta\lambda} = \mathrm{Da}\,\psi_P. \tag{2.69}$$

The results in the lower three panels of Figure 2.11 confirm that the scheme defined by Equations 2.67 to 2.69 exhibits a second-order convergence rate ($\mathcal{O} = 2$).

While it may be tempting to pursue ever higher-order schemes, one must recognize that higher-order methods generally entail greater computational cost. Although a higher-order method can achieve lower error for a fixed number of grid points, a lower-order method may reach comparable accuracy more efficiently by simply refining the grid. In practice, most commercial simulation packages employ first- and second-order methods, as these offer a favorable balance between accuracy and computational expense.[27]

[27] In practice, it is advisable to test which method best suits your specific problem. Also consider whether additional speed actually matters: improving an algorithm's runtime from 1 s to 0.1 s may not justify significant implementation effort if the original computation was already sufficiently fast.

2.6 Exercises

Exercise 2.1

a) Construct a finite difference model (FDM) for a plug-flow reactor (PFR) using an equidistant grid of points at

$$\vec{\lambda} = (0.1, 0.3, 0.5, 0.7, 0.9). \tag{2.70}$$

Use a two-point forward difference stencil such that

$$\frac{d\psi}{d\lambda}(\lambda_i) \approx \frac{\psi_i - \psi_{i-1}}{\lambda_i - \lambda_{i-1}} \tag{2.71}$$

Determine the the root-mean-squared error for $\mathrm{Da} = 5$.

b) Use a non-equidistant grid with grid points at

$$\vec{\lambda} = (0.05, 0.1, 0.15, 0.2, 0.9). \tag{2.72}$$

Determine the RMSE using the same discretization stencil as used in the previous subquestion and the same value for Da.

c) Which scheme is better? Provide a rationalization for your answer.

Exercise 2.2

a) Construct a Finite Volume Model for a PFR reactor using non-dimensionalized coordinates and for a first-order reaction. Its governing differential equation corresponds to

$$\frac{d\psi}{d\lambda} = -\mathrm{Da}\psi. \tag{2.73}$$

Take $\mathrm{Da} = 3$. For this model, use a non-equidistant grid of four grid cells with the following cell volumes

$$\vec{\Delta\lambda} = (0.1, 0.2, 0.3, 0.4) \tag{2.74}$$

Derive the coefficients of the finite volume discretization. Take specific care that for a non-uniform grid the cell volumes change per grid point. Furthermore, when you approximate the concentration at the cell boundaries, you need to use a so-called cantilever approximation where the contributions

of the central grid points depends inversely on the distance with respect to the cell boundary.

For example, for the concentration ψ_e, the following approximation needs to be used.

$$\psi_e \approx \frac{\Delta\lambda_E}{\Delta\lambda_E + \Delta\lambda_P}\psi_P + \frac{\Delta\lambda_P}{\Delta\lambda_E + \Delta\lambda_P}\psi_E \tag{2.75}$$

Likewise, for ψ_w, one uses

$$\psi_w \approx \frac{\Delta\lambda_W}{\Delta\lambda_W + \Delta\lambda_P}\psi_P + \frac{\Delta\lambda_P}{\Delta\lambda_W + \Delta\lambda_P}\psi_W. \tag{2.76}$$

b) Construct a secondary FVM model using the following cell volumes.

$$\vec{\Delta\lambda} = (0.05, 0.05, 0.1, 0.1, 0.15, 0.15, 0.2, 0.2) \tag{2.77}$$

Determine the concentration profile using this FVM and compare this profile both with the profile of the first model in the previous subquestion and with the analytical solution. Calculate the RMSE values and compare the two. Which of the two models performs better and why?

Exercise 2.3

a) Construct the finite difference coefficients for a 7-point equidistant central 2nd order stencil as shown schematically in Figure 2.12. **Note**: Although you can use an online generator to calculate these coefficients for you, the purpose of this exercise is to do it yourself.

b) Apply the stencil to calculate the 2nd derivative of $\cos(x)$ at $x = 0$. Compare your results to the analytical value.

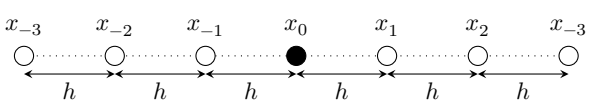

Figure 2.12: *Schematic depiction of a seven point stencil where the second-order derivative is approximated at the central point.*

.

3 NON-IDEAL TUBULAR REACTOR

Contents

3.1 Introduction

In this chapter, the finite volume method is applied to model a non-ideal continuous-flow reactor,[1] that is, a reactive system governed by the combined effects of convection, axial dispersion, and chemical reaction. It will be demonstrated that this system admits an analytical solution, and that the finite volume method can accurately reproduce this solution using only a small number of control volumes. Furthermore, it will be shown that the resulting concentration profile converges to the characteristic behaviors of the ideal plug-flow reactor and the continuously stirred tank reactor in the limits of vanishing and infinitely large axial dispersion, respectively.

[1] Specifically, the non-ideality arises from the fact that the tubular reactor does not exhibit perfect plug flow.

3.2 System definition and analytical solution

Consider a tubular, single phase, reactor with only a single reactive compound. The fluidic medium travels through the reactor at a uniform superficial speed v. The reactive compound is able to disperse through the reactor using an effective diffusion constant D. It should be noted that although the molecules diffuse through the fluidic medium, we here model the dispersion as being **superimposed** on the flow.[2] Finally, the reactive compound is consumed with a reaction rate corresponding to a first-order kinetic equation. For such a system, the governing partial differential equation is given by

$$\underbrace{\frac{dc}{dt}}_{\text{rate of change}} = \underbrace{D\frac{d^2c}{dx^2}}_{\text{diffusion}} - \underbrace{v\frac{dc}{dx}}_{\text{convection}} + \underbrace{r}_{\text{reaction}} \tag{3.1}$$

[2] This difference is important. Let me explain it by means of a short analogy. Suppose we have a train with drunk passengers. We can either model the random movement of the passengers with respect to the train or with respect to the track. When we superimpose the diffusion, we do the latter.

It is insightful to transform this system into its dimensionless representation by introduction of the following coordinate transformation

$$x \rightarrow \lambda = \frac{x}{L} \tag{3.2}$$

$$c \rightarrow \psi = \frac{c}{c_0} \tag{3.3}$$

We furthermore assume that the reactor is operated at steady-state, by which the time-derivative in Equation 3.1 equals zero. By furthermore dividing Equation 3.1 by $v\frac{c_0}{L}$, the following expression is obtained

$$\underbrace{\frac{D}{vL}}_{1/\,\mathrm{Pe}} \frac{d^2\psi}{d\lambda^2} - \frac{d\psi}{d\lambda} - k\underbrace{\frac{L}{v}}_{\mathrm{Da}}\psi = 0, \tag{3.4}$$

which hosts two dimensionless numbers Pe and Da which are conceptually described as[3]

[3] These two dimensionless numbers are known as the Péclet and Damköhler numbers.

$$\mathrm{Pe} = \frac{\text{advective transport rate}}{\text{diffusive transport rate}} \tag{3.5}$$

and

$$\mathrm{Da} = \frac{\text{reactive rate}}{\text{convective mass transport rate}}. \tag{3.6}$$

Because Equation 3.4 corresponds to a second-order ordinary differential equation, two boundary conditions need to be introduced to solve for ψ. These boundary conditions are known in the literature as the Danckwerts boundary conditions.[3] Under these conditions, it is assumed that the flow of concentration just before the inlet should equal net flow of concentration due to convection and diffusion just after the inlet, which is represented by the following identity

$$\left(\psi - \frac{1}{\mathrm{Pe}}\frac{d\psi}{d\lambda}\right)\Big|_{\lambda=0} = 1. \tag{3.7}$$

Furthermore, it is assumed that there is no convective flow at the end of the reactor, which gives

$$\frac{d\psi}{d\lambda}\Big|_{\lambda=1} = 0. \tag{3.8}$$

The ordinary differential equation Equation 3.4 has the following generalized solution[4]

[4] It is not straightforward to find this solution, although it is easy to verify that this solution is a valid solution and I warmly invite you to convince yourself of this. If you are more mathematically adventurous, an elegant way to find this solution is by means of a Laplace transformation.

$$\psi = C_1 \exp\left(\left(\frac{1+\beta}{2\alpha}\right)\lambda\right) + C_2\left(\left(\frac{1-\beta}{2\alpha}\right)\lambda\right), \tag{3.9}$$

wherein C_1 and C_2 are integration constants that can be found by application of the boundary conditions and α and β are given by

$$\alpha = \frac{1}{\mathrm{Pe}} \tag{3.10}$$

and

$$\beta = \sqrt{1 + 4\frac{\mathrm{Da}}{\mathrm{Pe}}}. \tag{3.11}$$

By application of these boundary conditions, the solution is given by[5]

$$\boxed{\psi(\lambda) = \frac{\exp\left(\frac{\mathrm{Pe}}{2}(1-\beta)\,\lambda\right) + \left(\frac{\beta-1}{\beta+1}\right)\exp\left(\frac{\mathrm{Pe}}{2}\left[(1+\beta)\,\lambda - 2\beta\right]\right)}{\frac{1}{2}(\beta+1) - \frac{(\beta-1)^2}{2(\beta+1)}\exp\left(-\beta\,\mathrm{Pe}\right)}}, \tag{3.12}$$

which is equivalent to the following solution[6]

$$\psi(\lambda) = \frac{2\exp\left(\frac{\mathrm{Pe}\,\lambda}{2}\right)\left[\beta\cosh\left(\frac{\mathrm{Pe}\,\beta}{2}(1-\lambda)\right) + \sinh\left(\frac{\mathrm{Pe}\,\beta}{2}(1-\lambda)\right)\right]}{(\beta^2+1)\sinh\left(\frac{\mathrm{Pe}\,\beta}{2}\right) + 2\beta\cosh\left(\frac{\mathrm{Pe}\,\beta}{2}\right)}. \tag{3.13}$$

[5] I do not expect you to derive this yourself, nor do you have any particular reason to.

[6] Just mentioning it for all the hyperbolic function afficionados.

3.3 Finite volume approximation

In the preceding sections, we have established the governing dimensionless equation for the generalized continuous-flow reactor. To obtain a practical numerical solution for this equation, we now introduce the finite volume method (FVM). The essence of this approach lies in dividing the reactor domain into a number of discrete control volumes and applying the conservation principle to each one individually. By integrating the governing equation over these control volumes, and replacing the unknown fluxes at the interfaces by suitable approximations, a set of algebraic equations is obtained that can be solved for the concentration profile along the reactor. In what follows, we present the derivation of the finite volume formulation for the one-dimensional reactor system and identify the corresponding discretization coefficients.

By minimal rearrangement of Equation 3.4, the governing equation for the non-ideal flow reactor can be expressed as

$$\frac{1}{\mathrm{Pe}}\frac{d^2\psi}{d\lambda^2} - \frac{d\psi}{d\lambda} = \mathrm{Da}\,\psi. \tag{3.14}$$

The spatial domain of this function extends from $\lambda = 0$ to $\lambda = 1$, and is discretized into N uniformly sized control volumes. For each control volume, we integrate Equation 3.14, yielding

$$\int_{\mathrm{CV}} \left(\frac{1}{\mathrm{Pe}}\frac{d^2\psi}{d\lambda^2} - \frac{d\psi}{d\lambda}\right) dV = \int_{\mathrm{CV}} (\mathrm{Da}\,\psi)\, dV \tag{3.15}$$

Applying the divergence theorem (recognizing that this is a one-dimensional problem[7]) and substituting $dV = A_\perp\, d\lambda$, we obtain[8]

$$A_\perp\left(\frac{1}{\mathrm{Pe}}\frac{d\psi}{d\lambda}(\lambda_e) - \psi(\lambda_e) - \frac{1}{\mathrm{Pe}}\frac{d\psi}{d\lambda}(\lambda_w) + \psi(\lambda_w)\right) = \int_{\mathrm{CV}} (\mathrm{Da}\,\psi)\, A_\perp d\lambda. \tag{3.16}$$

[7] See Equation 2.25 on page 17.

[8] With the notation "$\frac{d\psi}{d\lambda}(\lambda_e)$", we indicate that the first derivative of ψ with respect to λ is evaluated at the point λ_e.

Solving for the integral on the right-hand side gives

$$A_\perp \left(\frac{1}{\mathrm{Pe}} \left(\left.\frac{d\psi}{d\lambda}\right|_e - \left.\frac{d\psi}{d\lambda}\right|_w \right) - \psi_e + \psi_w \right) = \mathrm{Da} \cdot \psi_P \cdot A_\perp \Delta\lambda \tag{3.17}$$

which, upon division by the cross-sectional area $A_\perp$, becomes

$$\left(\frac{1}{\mathrm{Pe}} \left(\left.\frac{d\psi}{d\lambda}\right|_e - \left.\frac{d\psi}{d\lambda}\right|_w \right) - \psi_e + \psi_w \right) = \mathrm{Da} \cdot \psi_P \cdot \Delta\lambda. \tag{3.18}$$

Because no explicit information is available at the control-volume faces, approximations must be introduced to estimate ψ_e and ψ_w, as well as their first derivatives with respect to λ. The values of ψ_e and ψ_w have already been defined through linear interpolation, as shown in Equations 2.29 and 2.30. For the first derivatives, we employ midpoint discretization:

$$\left.\frac{d\psi}{d\lambda}\right|_e = \frac{\psi_E - \psi_P}{\Delta\lambda} \tag{3.19}$$

and

$$\left.\frac{d\psi}{d\lambda}\right|_w = \frac{\psi_P - \psi_W}{\Delta\lambda}. \tag{3.20}$$

Substituting these approximations into Equation 3.18 gives

$$\frac{1}{\mathrm{Pe}} \left(\frac{\psi_E - \psi_P}{\Delta\lambda} - \frac{\psi_P - \psi_W}{\Delta\lambda} \right) - \frac{\psi_E + \psi_P}{2} + \frac{\psi_W + \psi_P}{2} = \mathrm{Da} \cdot \psi_P \cdot \Delta\lambda \tag{3.21}$$

from which the constants a_W, a_E, a_P, and S_P can be directly derived for a central control volume. For control volumes located at the system boundaries, the derivation must be restarted from Equation 3.18.

At the reactor inlet, application of Equation 3.7 to Equation 3.18 yields

$$\left(\frac{1}{\mathrm{Pe}} \left.\frac{d\psi}{d\lambda}\right|_e - \psi_e \right) = \mathrm{Da} \cdot \psi_P \cdot \Delta\lambda - 1 \tag{3.22}$$

which, using the known sampling points, becomes

$$\left(\frac{1}{\mathrm{Pe}} \frac{\psi_E - \psi_P}{\Delta\lambda} - \frac{\psi_E + \psi_P}{2} \right) = \mathrm{Da} \cdot \psi_P \cdot \Delta\lambda - 1. \tag{3.23}$$

For the control volume at the outlet, application of Equation 3.8 to Equation 3.18 yields

$$\left(\frac{1}{\mathrm{Pe}} \left(- \left.\frac{d\psi}{d\lambda}\right|_w \right) - \psi_e + \psi_w \right) = \mathrm{Da} \cdot \psi_P \cdot \Delta\lambda. \tag{3.24}$$

At this point, $\left.\frac{d\psi}{d\lambda}\right|_e$ cannot be approximated using ψ_E since that point lies outside the system domain. Therefore, we introduce an additional

assumption consistent with the general plug-flow reactor, setting $\psi_e = \psi_P$, which yields

$$\frac{1}{\mathrm{Pe}}\left(-\frac{\psi_P - \psi_W}{\Delta\lambda}\right) - \frac{\psi_P + \psi_P}{2} + \frac{\psi_W + \psi_P}{2} = \mathrm{Da}\cdot\psi_P\cdot\Delta\lambda. \tag{3.25}$$

The resulting finite volume discretization coefficients are summarized in Table 3.1.

Table 3.1: *Finite volume discretization coefficients for a tubular plug-flow reactor with convection, dispersion, and a first-order reaction.*

Terms	a_W	a_P	a_E	b
$i = 0$	0	$-\frac{1}{\mathrm{Pe}\,\Delta\lambda} - \frac{1}{2} - \mathrm{Da}\,\Delta\lambda$	$\frac{1}{\mathrm{Pe}\,\Delta\lambda} - \frac{1}{2}$	-1
$0 < i < N-1$	$\frac{1}{\mathrm{Pe}\,\Delta\lambda} + \frac{1}{2}$	$-\frac{2}{\mathrm{Pe}\,\Delta\lambda} - \mathrm{Da}\,\Delta\lambda$	$\frac{1}{\mathrm{Pe}\,\Delta\lambda} - \frac{1}{2}$	0
$i = N-1$	$\frac{1}{\mathrm{Pe}\,\Delta\lambda} + \frac{1}{2}$	$-\frac{1}{\mathrm{Pe}\,\Delta\lambda} - \frac{1}{2} - \mathrm{Da}\,\Delta\lambda$	0	0

With these coefficients established, the equations can be readily implemented in a computational script to evaluate the concentration as a function of position within the reactor.[9] The resulting concentration profile, shown in Figure 3.1 for $N = 5$ control volumes and $\mathrm{Da} = \mathrm{Pe} = 1$, demonstrates the accuracy of the finite volume approximation.

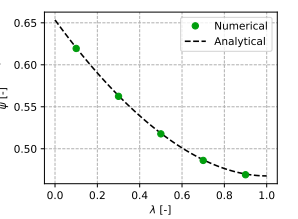

Figure 3.1: *Dimensionless concentration profile of a generalized continuous reactor using* $\mathrm{Da} = 1$ *and* $\mathrm{Pe} = 1$.

[9] The implementation script is available at https://bit.ly/3gR4oCx.

Having established the model, we can now examine the effect of the Péclet number on the reactor behavior. Figure 3.2 shows this dependency: at low Péclet numbers, the solution approaches that of an ideal plug-flow reactor, while increasing the Péclet number flattens the profile. In the limit of infinite Pe, the concentration distribution becomes uniform, as expected for a continuously stirred tank reactor.

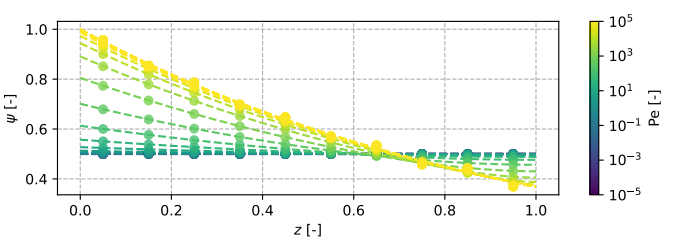

Figure 3.2: *Dimensionless concentration profile of a generalized continuous reactor using* $\mathrm{Da} = 1$ *at different values for the Péclet number.*

These limiting cases are fully consistent with theoretical expectations. As $\mathrm{Pe} \to \infty$, Equation 3.14 reduces to the differential equation of a

plug-flow reactor (Equation 2.2). Conversely, when $\mathrm{Pe} \to 0$, the equation degenerates into the algebraic form

$$1 = (1 + \mathrm{Da})\,\psi \tag{3.26}$$

which has the solution[10]

$$\psi = \frac{1}{1 + \mathrm{Da}}. \tag{3.27}$$

[10] This is the familiar dimensionless steady-state solution for a continuously stirred tank reactor.

From Figure 3.2, it can also be observed that with as few as ten control volumes, the numerical solution provides an excellent approximation of the analytical result.

To conclude this chapter, we assess the accuracy of the finite volume discretization. Following the same procedure described in Section 2.5, the mean absolute percentage error (MAPE) (Equation 2.65) is used as the error metric. The analysis, performed as a function of the Péclet number, is summarized in Figure 3.3.

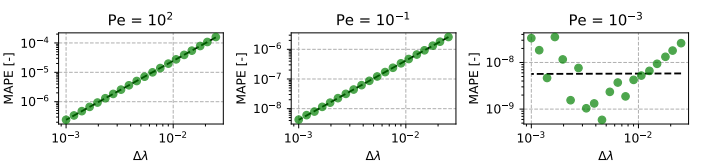

Figure 3.3: *Error analysis of the finite volume model as function of the Péclet number.*

From Figure 3.3, it can be seen that for sufficiently large Pe, the method achieves second-order accuracy. However, a deviation is observed for small Pe values. As discussed earlier, low Péclet numbers correspond to dominant diffusion, causing the tubular reactor to behave as a CSTR. In this limit, the governing partial differential equation (Equation 3.1) reduces to an algebraic balance (Equation 1.31). Accurately describing such a system requires only a single control volume; increasing or decreasing the number of volumes has little effect on the overall error. Indeed, as shown in the right-hand graph of Figure 3.3, the error becomes essentially independent of the step size $\Delta\lambda$ and remains extremely small.[11]

[11] Note that the mean error lies within the parts-per-billion range.

3.4 Exercises

Exercise 3.1

a) Construct a finite volume model (FVM) for a generalized tubular reactor incorporating diffusion, convection and a first-order reaction according to the following non-dimensionalized design equation

$$\frac{1}{\mathrm{Pe}}\frac{d^2\psi}{d\lambda^2} - \frac{d\psi}{d\lambda} - \mathrm{Da}\psi = 0. \tag{3.28}$$

Explore the effect of varying Péclet number between $10^{-5} \leq \mathrm{Pe} 10^{5}$. Use Danckwerts boundary conditions. Take $N = 10$ equidistant control volumes and $\mathrm{Da} = 1$. Verify your simulation results with the analytical solution.

b) To which prototypical reactor models do the concentration profiles correspond in the limit of $\mathrm{Pe} \to 0$ and $\mathrm{Pe} \to \infty$? Determine the analytical solutions for these two reactor models and compare these with the simulation results of the previous subquestion.

4 ORTHOGONAL CURVILINEAR COORDINATES

Contents

4.1 Introduction

In geometry, *curvilinear coordinates* refer to coordinate systems defined in Euclidean space,[1] where the coordinate lines are not necessarily straight but may instead be curved. Such coordinates can be constructed from a Cartesian system through a locally invertible transformation, meaning a one-to-one mapping that exists in a neighborhood around each point. Consequently, any point specified in Cartesian coordinates can be converted into its corresponding curvilinear coordinates, and vice versa.

[1] That is, the familiar space of everyday experience, in contrast to non-Euclidean spaces, which exhibit distinct properties such as the curious fact that the sum of the interior angles of a triangle may differ from 180 degrees.

When the curvilinear coordinate lines are locally orthogonal, meaning that at every point in space the associated basis vectors intersect at right angles, the system is said to be *orthogonal*. Local orthogonality is generally sufficient for most analyses, although some coordinate systems are globally orthogonal, where the basis vectors remain mutually perpendicular throughout the entire domain. The Cartesian coordinate system is the most straightforward example of a globally orthogonal system. Common orthogonal curvilinear coordinate systems used in engineering include the cylindrical and spherical coordinate systems.

Employing a curvilinear coordinate system can greatly simplify the formulation of certain physical problems compared to Cartesian coordinates. In particular, when the boundaries of a system conform to the coordinate surfaces of a given curvilinear system, the associated governing equations and boundary conditions often become far easier to handle. For instance, describing a cylindrical reactor in cylindrical coordinates is considerably

more natural than attempting the same in Cartesian coordinates, since the reactor walls align perfectly with the coordinate surfaces.[2]

In many chemical reaction engineering textbooks, the most common coordinate systems and their properties are simply stated. You are likely already familiar with the cylindrical and spherical coordinate systems and know where to *find* the standard expressions for the gradient, the Laplacian, the differential surface area element, and the Jacobian.[3] However, you may encounter a problem where none of these conventional systems naturally fit the geometry or boundary conditions of your system. In such cases, defining your own coordinate system can lead to substantial simplification. In this chapter, I will show how this can be achieved and why orthogonal curvilinear coordinates are particularly advantageous for this purpose.

[2] If you doubt this, try defining the boundary conditions of a cylindrical reactor in Cartesian coordinates. It can be done, but it is far from convenient.

[3] The Jacobian is also referred to as the differential volume element.

4.2 Coordinates, basis and vectors

To describe a space, we employ basis vectors together with their corresponding coordinates. For a three-dimensional space, three basis vectors and three coordinates are required. The simplest example is the standard Cartesian space, in which the basis vectors are independent of position and span the tangent space at every point. These basis vectors are also normalized, meaning that each has unit length.

> **Warning**
>
> In this chapter, I use a slightly different notation than what you may be accustomed to. This choice is made to remain consistent with the literature on this topic. The main source of potential confusion is the use of superscript indices to denote coordinates, which can resemble exponents. In this chapter, the context should make it clear which interpretation applies, but it is worth keeping in mind.

The Cartesian basis vectors are given by

$$\hat{e}_1 = (1, 0, 0)\,, \tag{4.1}$$

$$\hat{e}_2 = (0, 1, 0)\,, \tag{4.2}$$

$$\hat{e}_3 = (0, 0, 1)\,, \tag{4.3}$$

from which it follows[4] that

$$\hat{e}_i \cdot \hat{e}_j = \delta_{ij}, \tag{4.4}$$

where δ_{ij} is the Kronecker delta, defined as

$$\delta_{ij} = \begin{cases} 1, & \text{if } i = j, \\ 0, & \text{otherwise.} \end{cases} \tag{4.5}$$

[4] See Equation 4.4, which shows that the basis vectors are locally orthogonal and normalized. In the special case of the Cartesian coordinate system, they are also globally orthogonal.

The Cartesian coordinates are given[5] by $\{x^1, x^2, x^3\} = \{x, y, z\}$. The position vector $\vec{r} \in \mathbb{R}^3$ can therefore be written as

$$\vec{r} = x^1 \hat{e}_1 + x^2 \hat{e}_2 + x^3 \hat{e}_3. \tag{4.6}$$

Having established how coordinates and basis vectors define positions in space, we can now extend this framework to describe how functions vary within that space. To do so, we introduce the differential and integral elements that enable operations such as differentiation and integration in a given coordinate system.

[5] As a kind reminder, do not confuse the superscript indices with powers; they are **indices**.

4.3 Elements for differentiation and integration

Engineering applications frequently require the evaluation of derivatives and integrals within a given spatial domain. In this book, and particularly in the context of the finite volume method, we primarily make use of the gradient and the Laplacian for differentiation, and of the differential surface and volume elements, dA and dV, for integration.

The gradient of a scalar function f with respect to the coordinates x^i and the basis vectors $\hat{e}_i$ of a coordinate system is defined as

$$\nabla f = \sum_i \hat{e}_i \frac{\partial f}{\partial x^i}. \tag{4.7}$$

In the Cartesian coordinate system, the gradient operator itself takes the familiar form

$$\begin{aligned} \nabla &= \sum_{i=1}^{3} \hat{e}_i \frac{\partial}{\partial x^i} && (4.8)\\ &= \hat{e}_1 \frac{\partial}{\partial x^1} + \hat{e}_2 \frac{\partial}{\partial x^2} + \hat{e}_3 \frac{\partial}{\partial x^3} && (4.9)\\ &= \hat{\imath} \frac{\partial}{\partial x} + \hat{\jmath} \frac{\partial}{\partial y} + \hat{k} \frac{\partial}{\partial z}. && (4.10) \end{aligned}$$

The *Laplacian* operator is defined as the divergence of the gradient,

$$\nabla^2 f = \nabla \cdot \nabla f, \tag{4.11}$$

which in Cartesian coordinates simplifies to

$$\nabla^2 = \sum_{i=1}^{3} \frac{\partial^2}{\partial (x^i)^2} = \frac{\partial^2}{\partial x^2} + \frac{\partial^2}{\partial y^2} + \frac{\partial^2}{\partial z^2}. \tag{4.12}$$

The differential volume element, whose scaling is determined by the Jacobian in curvilinear coordinates, is expressed in Cartesian form as

$$dV = dx^1\, dx^2\, dx^3 = \prod_{i=1}^{3} dx^i = dx\, dy\, dz, \tag{4.13}$$

and the differential surface area element is given by

$$dA^{ik} = dx^i\, dx^k, \quad \forall\ i \neq k, \tag{4.14}$$

where i and k each denote one of the three Cartesian coordinates.

Aside from the notation, these results should be familiar. They represent the standard expressions for differentiation and integration in Cartesian coordinates, yet with the definitions above we can now see how they can be systematically constructed from the underlying basis vectors and coordinates.

4.4 The metric tensor

Suppose we wish to describe **the same physical space**[6] using a different set of basis vectors $\{\hat{b}_1, \hat{b}_2, \hat{b}_3\}$ and coordinates $\{q_1, q_2, q_3\}$. To do so, we must determine new expressions for the differential and integral elements in this coordinate system. We begin by introducing a locally invertible transformation that expresses the position vector $\vec{r} \in \mathbb{R}^3$ in terms of the new coordinates as

$$\vec{r} = x^1(q^1, q^2, q^3)\hat{e}_1 + x^2(q^1, q^2, q^3)\hat{e}_2 + x^3(q^1, q^2, q^3)\hat{e}_3. \tag{4.15}$$

[6] This point is important. Describing a space with curvilinear coordinates instead of Cartesian ones is analogous to measuring with curved rulers rather than straight ones. As long as we know precisely how the rulers are curved, there is no loss of accuracy—in fact, the curved rulers may even simplify the description.

In this notation, $x^1(q^1, q^2, q^3)$ indicates that x^1 is a function of (q^1, q^2, q^3). To illustrate the process, we consider the spherical coordinate system, shown in Figure 4.1. The Cartesian coordinates (x, y, z) as functions of the spherical coordinates (ρ, ϕ, θ) are

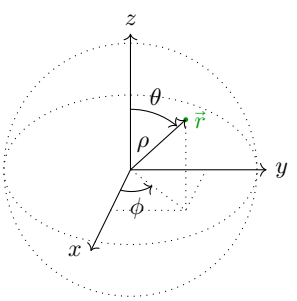

Figure 4.1: *Schematic depiction of the spherical coordinate system. Note that ϕ and θ correspond to the azimuthal and polar angles, respectively.*

$$x = \rho \cos\phi \sin\theta, \tag{4.16}$$

$$y = \rho \sin\phi \sin\theta, \tag{4.17}$$

$$z = \rho \cos\theta. \tag{4.18}$$

Substituting Equations 4.16 to 4.18 into Equation 4.15 gives

$$\vec{r} = (\rho \cos\phi \sin\theta)\hat{e}_1 + (\rho \sin\phi \sin\theta)\hat{e}_2 + (\rho \cos\theta)\hat{e}_3. \tag{4.19}$$

The Cartesian basis vectors can be obtained from

$$\hat{e}_i = \frac{\partial \vec{r}}{\partial x^i}, \tag{4.20}$$

and we can extend this definition to the new curvilinear coordinates, defining the *natural basis vectors*

$$\vec{h}_i = \frac{\partial \vec{r}}{\partial q^i}. \tag{4.21}$$

The differential position vector is therefore given by

$$d\vec{r} = \sum_{i=1}^{3} \frac{\partial \vec{r}}{\partial q^i} dq^i = \sum_{i=1}^{3} \vec{h}_i dq^i. \tag{4.22}$$

Each natural basis vector can be written as $\vec{h}_i = h_i \hat{b}_i$, where h_i are the *scaling factors*[7] and $\hat{b}_i$ are the unit basis vectors of the curvilinear coordinate system, such that

[7] The h_i are scalars that scale the local coordinate differentials.

$$\vec{r} = q^1 \hat{b}_1 + q^2 \hat{b}_2 + q^3 \hat{b}_3. \tag{4.23}$$

Applying these definitions to the spherical coordinate system, we obtain the scaling factors

$$\begin{aligned}
h_1 &= \left| \frac{\partial \vec{r}}{\partial \rho} \right| && (4.24)\\
&= |(\sin\theta\cos\phi)\,\hat{e}_1 + (\sin\theta\sin\phi)\,\hat{e}_2 + (\cos\theta)\,\hat{e}_3| && (4.25)\\
&= \sqrt{(\sin\theta\cos\phi)^2 + (\sin\theta\sin\phi)^2 + (\cos\theta)^2} && (4.26)\\
&= \sqrt{\sin^2\theta\left(\cos^2\phi + \sin^2\phi\right) + \cos^2\theta} && (4.27)\\
&= 1 && (4.28)
\end{aligned}$$

and

$$\begin{aligned}
h_2 &= \left| \frac{\partial \vec{r}}{\partial \phi} \right| && (4.29)\\
&= |(\rho\sin\theta\sin\phi)\,\hat{e}_1 + (-\rho\sin\theta\cos\phi)\,\hat{e}_2| && (4.30)\\
&= \sqrt{(\rho\sin\theta\sin\phi)^2 + (-\rho\sin\theta\cos\phi)^2} && (4.31)\\
&= \sqrt{\left(\rho^2\sin^2\theta\right)\left(\sin^2\phi + \cos^2\phi\right)} && (4.32)\\
&= \rho\sin\theta && (4.33)
\end{aligned}$$

and finally

$$\begin{aligned}
h_3 &= \left| \frac{\partial \vec{r}}{\partial \theta} \right| && (4.34)\\
&= |(\rho\cos\theta\cos\phi)\,\hat{e}_1 + (\rho\cos\theta\sin\phi)\,\hat{e}_2 + (-\rho\sin\theta)\,\hat{e}_3| && (4.35)\\
&= \sqrt{(\rho\cos\theta\cos\phi)^2 + (\rho\cos\theta\sin\phi)^2 + (-\rho\sin\theta)^2} && (4.36)\\
&= \sqrt{(\rho^2\cos^2\theta)\left(\cos^2\phi + \sin^2\phi\right) + \rho^2\sin^2\theta} && (4.37)\\
&= \rho. && (4.38)
\end{aligned}$$

The corresponding unit basis vectors are

$$\hat{b}_1 = \hat{\rho} = (\sin\theta\cos\phi)\hat{e}_1 + (\sin\theta\sin\phi)\hat{e}_2 + (\cos\theta)\hat{e}_3, \tag{4.39}$$

$$\hat{b}_2 = \hat{\phi} = (-\sin\phi)\hat{e}_1 + (\cos\phi)\hat{e}_2, \tag{4.40}$$

$$\hat{b}_3 = \hat{\theta} = (\cos\theta\cos\phi)\hat{e}_1 + (\cos\theta\sin\phi)\hat{e}_2 - (\sin\theta)\hat{e}_3, \tag{4.41}$$

[8] Trust me, I am an engineer.

for which it can be verified through straightforward algebra that[8]

$$\hat{b}_i \cdot \hat{b}_j = \delta_{ij}. \tag{4.42}$$

From the natural basis vectors, we construct the *metric tensor* g, whose components are defined as

$$g_{ij} = \vec{h}_i \cdot \vec{h}_j. \tag{4.43}$$

[9] Note that $g_{ii} = h_i^2$; the diagonal elements of the metric tensor are the squares of the scaling factors.

For the spherical coordinate system, this gives[9]

$$g = \begin{pmatrix} 1 & 0 & 0 \\ 0 & \rho^2\sin^2\theta & 0 \\ 0 & 0 & \rho^2 \end{pmatrix}. \tag{4.44}$$

Note

The most important expressions from this section, used to construct differential and integral elements, have been boxed for convenience.

The metric tensor plays a central role in geometry, as it defines how distances, angles, and volumes are measured in a given coordinate system. For example, when integrating over a space described by g_{ij}, the differential volume element must include the metric's determinant,[10] giving

[10] This illustrates how the determinant of a matrix encodes a volume-scaling property.

$$\boxed{dV = \sqrt{\det(g)}\prod_i dq^i} = \rho^2\sin\theta\, d\rho\, d\theta\, d\phi. \tag{4.45}$$

To show an example, integrating dV over $\rho \in (0, R)$, $\phi \in (0, 2\pi)$, and $\theta \in (0, \pi)$ yields

$$V = \iiint_V dV = \int_0^R \rho^2 d\rho \int_0^\pi \sin\theta d\theta \int_0^{2\pi} d\phi \tag{4.46}$$

$$= \frac{4\pi R^3}{3}, \tag{4.47}$$

which corresponds to the volume of a sphere of radius R.

The metric tensor also defines differential surface elements dA, which in general are given by

$$dA^{(ik)} = \sqrt{g_{ii}g_{kk} - g_{ik}g_{ki}}\, dq^i dq^k. \tag{4.48}$$

For orthogonal coordinate systems (where the metric tensor is diagonal), this simplifies to

$$\boxed{dA^{(ik),\perp} = \sqrt{g_{ii}g_{kk}}\, dq^i dq^k = h_i h_k\, dq^i dq^k}. \tag{4.49}$$

For instance, the surface element at $\rho = R$ for $\phi \in (0, 2\pi)$ and $\theta \in (0, \pi)$ is

$$dA^{(\phi,\theta)} = \rho^2 \sin\theta\, d\theta\, d\phi. \tag{4.50}$$

Integrating this surface element gives

$$A_{\rho=R} = \iint_A dA = R^2 \int_0^{\pi} \sin\theta d\theta \int_0^{2\pi} d\phi \tag{4.51}$$

$$= 4\pi R^2, \tag{4.52}$$

which is the surface area of a sphere.

The metric tensor can also be used to construct the gradient operator for an orthogonal curvilinear coordinate system:

$$\nabla f = \sum_i \frac{1}{h_i} \frac{\partial f}{\partial q^i} \hat{b}_i. \tag{4.53}$$

For the spherical coordinate system, this becomes

$$\boxed{\nabla_{\rho,\phi,\theta} = \hat{\rho}\frac{\partial}{\partial\rho} + \frac{\hat{\phi}}{\rho\sin\theta}\frac{\partial}{\partial\phi} + \frac{\hat{\theta}}{\rho}\frac{\partial}{\partial\theta}}. \tag{4.54}$$

Similarly, the Laplacian operator can be expressed in terms of the scaling factors as

$$\boxed{\nabla^2 = \frac{1}{\prod_j h_j} \sum_i \frac{\partial}{\partial q^i}\left(\frac{\prod_j h_j}{h_i^2}\frac{\partial}{\partial q^i}\right)}. \tag{4.55}$$

Since $g_{ii} = h_i^2$, substitution for the spherical coordinate system yields

$$\boxed{\nabla^2_{\rho,\phi,\theta} = \frac{1}{\rho^2}\frac{\partial}{\partial\rho}\left(\rho^2\frac{\partial}{\partial\rho}\right) + \frac{1}{\rho^2\sin^2\theta}\frac{\partial^2}{\partial\phi^2} + \frac{1}{\rho^2\sin\theta}\frac{\partial}{\partial\theta}\left(\sin\theta\frac{\partial}{\partial\theta}\right)}. \tag{4.56}$$

In conclusion, we have demonstrated that all differential and integral elements of the spherical coordinate system can be systematically derived from its metric tensor, which itself originates from the one-to-one transformation between the spherical and Cartesian coordinate systems.

Note

Vector vs. scalar output. In an orthogonal curvilinear system with scale factors h_i and unit basis vectors $\hat{b}_i$, the gradient of a scalar field f is a vector. The basis vectors must appear explicitly:

$$\nabla f = \sum_i \frac{\hat{b}_i}{h_i} \frac{\partial f}{\partial q^i}. \tag{4.57}$$

By contrast, the Laplacian of a scalar field is a scalar:

$$\nabla^2 f = \frac{1}{\prod_j h_j} \sum_i \frac{\partial}{\partial q^i} \left(\frac{\prod_j h_j}{h_i^2} \frac{\partial f}{\partial q^i} \right). \tag{4.58}$$

The distinction holds under the assumptions used in this section, namely that f is a scalar field and the coordinates are orthogonal with $g_{ii} = h_i^2$.

4.5 Elliptic cylindrical coordinates

To conclude upon this chapter, I will show you one more derivation for a coordinate system you are most likely not very familiar with. This coordinate system pertains to elliptic cylindrical coordinates and can, for example, be used to describe the geometry of a catalytic converter whose outer walls are well represented by these coordinates.

The transformation between the elliptic cylindrical coordinates (μ, ν, z) and the Cartesian coordinates is given by

$$x = a \cosh \mu \cos \nu \tag{4.59}$$

$$y = a \sinh \mu \sin \nu \tag{4.60}$$

$$z = z, \tag{4.61}$$

wherein a denotes the focal distance, i.e. the distance from the origin to each of the two foci located at $(\pm a, 0, 0)$. The semi-major axis therefore coincides with the x-axis and the semi-minor axis with the y-axis.

Surfaces of constant $\mu = p$ correspond to ellipses in the xy-plane. For such an ellipse, the Cartesian coordinates satisfy

$$\frac{x^2}{(a \cosh p)^2} + \frac{y^2}{(a \sinh p)^2} = 1, \tag{4.62}$$

from which it follows that the semi-major and semi-minor axes are given by

$$A = a \cosh p \tag{4.63}$$

$$B = a \sinh p. \tag{4.64}$$

Hence, A and B represent the lengths of the semi-axes of the ellipse, while a is the focal distance, related to them through

$$A^2 - B^2 = a^2. \tag{4.65}$$

Since the elliptic cylindrical coordinate system is orthogonal, we can construct the metric tensor directly from the scale factors:

$$g = \begin{pmatrix} h_\mu^2 & 0 & 0 \\ 0 & h_\nu^2 & 0 \\ 0 & 0 & h_z^2 \end{pmatrix}. \tag{4.66}$$

The scale factors are obtained from the natural basis vectors $\vec{h}_i = \partial\vec{r}/\partial q^i$:

$$h_\mu = \left\| \frac{\partial}{\partial \mu} \left[(a\cosh\mu\cos\nu)\,\hat{e}_1 + (a\sinh\mu\sin\nu)\,\hat{e}_2 + z\,\hat{e}_3 \right] \right\| \tag{4.67}$$

$$= \sqrt{(a\sinh\mu\cos\nu)^2 + (a\cosh\mu\sin\nu)^2} \tag{4.68}$$

$$= a\sqrt{\sinh^2\mu\cos^2\nu + \cosh^2\mu\sin^2\nu} = a\sqrt{\sinh^2\mu + \sin^2\nu}, \tag{4.69}$$

where we used $\cosh^2\mu = 1 + \sinh^2\mu$. Similarly,

$$h_\nu = \left\| \frac{\partial}{\partial \nu} \left[(a\cosh\mu\cos\nu)\,\hat{e}_1 + (a\sinh\mu\sin\nu)\,\hat{e}_2 + z\,\hat{e}_3 \right] \right\| \tag{4.70}$$

$$= \sqrt{(-a\cosh\mu\sin\nu)^2 + (a\sinh\mu\cos\nu)^2} \tag{4.71}$$

$$= a\sqrt{\cosh^2\mu\sin^2\nu + \sinh^2\mu\cos^2\nu} = a\sqrt{\sinh^2\mu + \sin^2\nu}, \tag{4.72}$$

using the same identity.
Finally,

$$h_z = \left\| \frac{\partial}{\partial z} \left[(a\cosh\mu\cos\nu)\,\hat{e}_1 + (a\sinh\mu\sin\nu)\,\hat{e}_2 + z\,\hat{e}_3 \right] \right\| = \|\hat{e}_3\| = 1. \tag{4.73}$$

Thus, the differential volume element is

$$dV = a^2\left(\sinh^2\mu + \sin^2\nu\right)\,d\mu\,d\nu\,dz. \tag{4.74}$$

The differential surface area element for a surface perpendicular to the z-direction is given by

$$dA^{(\mu,\nu)} = a^2\left(\sinh^2\mu + \sin^2\nu\right)\,d\mu\,d\nu. \tag{4.75}$$

Using the above element, we can readily calculate the surface area of an ellipse bounded by $\mu \in (0, p)$ and $\nu \in (0, 2\pi)$, wherein p is given by

$$p = \cosh^{-1}\left(\frac{A}{a}\right) = \sinh^{-1}\left(\frac{B}{a}\right). \tag{4.76}$$

Integration of the differential surface area element with these bounds yields

$$S = \iint_A dA \tag{4.77}$$

$$= \int_0^p \left[\int_0^{2\pi} a^2 \left(\sinh^2 \mu + \sin^2 \nu \right) d\nu \right] d\mu \tag{4.78}$$

$$= \int_0^p \left[a^2 \left(2\pi \sinh^2 \mu + \pi \right) \right] d\mu \tag{4.79}$$

$$= 2\pi a^2 \int_0^p \left(\sinh^2 \mu + \tfrac{1}{2} \right) d\mu \tag{4.80}$$

$$= 2\pi a^2 \int_0^p \left(\tfrac{1}{2} \cosh 2\mu \right) d\mu \tag{4.81}$$

$$= 2\pi a^2 \left(\tfrac{1}{4} \sinh 2p \right) \tag{4.82}$$

$$= \pi a^2 \sinh p \cosh p \tag{4.83}$$

$$= \pi AB. \tag{4.84}$$

This result corresponds to the surface area of an ellipse with semi-major and semi-minor axes A and B, respectively. This result can be readily extended to find the volume of an elliptic cylinder, which yields

$$V = \pi ABL, \tag{4.85}$$

where L denotes the length of the cylinder.

Having established the scale factors and the orthogonality of the elliptic cylindrical coordinates, we now construct the differential operators needed for analysis in this system. We begin with the gradient of a scalar field $f(\mu, \nu, z)$. In any orthogonal curvilinear coordinate system with scale factors h_i and unit basis vectors $\hat{b}_i$, the gradient is given by

$$\nabla f = \sum_i \frac{\hat{b}_i}{h_i} \frac{\partial f}{\partial q^i}. \tag{4.86}$$

Specializing to the elliptic cylindrical coordinates, where $h_\mu = h_\nu = a\sqrt{\sinh^2 \mu + \sin^2 \nu}$ and $h_z = 1$, we obtain

$$\nabla f = \frac{\hat{b}_\mu}{a\sqrt{\sinh^2 \mu + \sin^2 \nu}} \frac{\partial f}{\partial \mu} + \frac{\hat{b}_\nu}{a\sqrt{\sinh^2 \mu + \sin^2 \nu}} \frac{\partial f}{\partial \nu} + \hat{b}_z \frac{\partial f}{\partial z}. \tag{4.87}$$

Next, we turn to the Laplacian. For orthogonal coordinates, the Laplacian of a scalar field follows from the scale factors via

$$\nabla^2 f = \frac{1}{h_\mu h_\nu h_z} \left[\frac{\partial}{\partial \mu} \left(\frac{h_\nu h_z}{h_\mu} \frac{\partial f}{\partial \mu} \right) + \frac{\partial}{\partial \nu} \left(\frac{h_\mu h_z}{h_\nu} \frac{\partial f}{\partial \nu} \right) + \frac{\partial}{\partial z} \left(\frac{h_\mu h_\nu}{h_z} \frac{\partial f}{\partial z} \right) \right]. \tag{4.88}$$

Substituting $h_\mu = h_\nu = a\sqrt{\sinh^2\mu + \sin^2\nu}$ and $h_z = 1$ simplifies this expression to

$$\nabla^2 f = \frac{1}{a^2(\sinh^2\mu + \sin^2\nu)}\left(\frac{\partial^2 f}{\partial\mu^2} + \frac{\partial^2 f}{\partial\nu^2}\right) + \frac{\partial^2 f}{\partial z^2}. \tag{4.89}$$

These formulas provide the gradient and Laplacian in elliptic cylindrical coordinates in terms of the scale factors and basis, which completes the set of differential elements needed for subsequent analysis.

.

5 REACTION-DIFFUSION IN SPHERICAL PELLETS

Contents

5.1 Introduction

A common type of catalytic reactor is wherein a tubular vessel is loaded with porous catalyst pellets. Typically these pellets are a few millimeters in size. The reactive medium can enter these pellets through porous channels. The walls of these porous channels are decorated with nanometer-sized metallic particles. These metallic nanoparticles are the active ingredient of the catalyst and on the active sites harbored by these metallic nanoparticles, the catalytic conversion takes place. The products so formed leave the catalyst pellet by the same route as by which the reactants entered the pellet. Because of the size of the porous channels, the physical process by which the reactants migrate through the pellet is by diffusion rather than by convection. As such, in the absence of convection, the concentration profile inside these pellets can be modelled as a reaction-diffusion system.

In this chapter, we will construct a numerical model to describe such reaction-diffusion systems. We start by constructing analytical solutions as these are crucial for model verification. Next, a finite volume representation is built. Finally, we use the model to identify limiting situations due to temperature effects.

5.2 Analytical solution

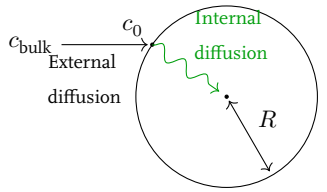

Figure 5.1: *Schematic depiction of the catalyst pellet.*

Consider a spherical pellet as schematically depicted in Figure 5.1. We assume that external diffusion limitations from the bulk concentration towards the external pellet surface are negligible and that there are only concentration gradients in the radial direction.[1] The fundamental equation that describes reaction and diffusion for such a spherical system is then given by[2]

$$D\nabla^2 c = kc, \tag{5.1}$$

wherein we use ∇^2 to represent the second derivative.[3]

Equation 5.1 is associated with two boundary conditions, corresponding to a Dirichlet boundary conditions at the particle edge

$$c|_{r=R} = c_0 \tag{5.2}$$

and a Neumann boundary condition at the particle center

$$\nabla c|_{r=0} = 0 \tag{5.3}$$

The exact definition of the Laplacian as given in Equation 5.1 depends on the coordinate system. Here we employ spherical coordinates for which we have derived that the Laplacian is given by Equation 4.55.[4] Since there are no concentration gradients in the azimuthal or polar direction, the Laplacian is given by

$$\nabla^2 c = \frac{1}{r^2}\frac{\partial}{\partial r}\left(r^2 \frac{\partial c}{\partial r}\right). \tag{5.4}$$

Similar to the previous chapters, we would like to non-dimensionalize the above equation. Herein, we use the following coordinate transformation

$$\psi = \frac{c}{c_0}, \tag{5.5}$$

wherein c_0 is the concentration at the exterior of the particle system[5] and

$$\lambda = \frac{r}{R}, \tag{5.6}$$

wherein R is the radius of the spherical pellet and r the radial distance with respect to the center of the pellet. To perform the non-dimensionalization, we have to investigate how the (radial) Laplacian as given by Equation 5.4 transform under the coordinate transformation. To do so, we make ourselves aware of the following identity

$$\frac{\partial}{\partial r} = \frac{\partial}{\partial \lambda}\frac{\partial \lambda}{\partial r}. \tag{5.7}$$

[1] The system is highly symmetric and one would expect only concentration gradients to occur in the radial direction.

[2] Here assuming a first-order reaction and operating under steady-state conditions.

[3] The operator ∇^2 is sometimes called the Laplacian. The advantage of using ∇^2 to represent the Laplacian is that this notation is agnostic to the type of coordinate system you use to represent the physical situation. As such, Equation 5.1 would look exactly the same for a cartesian or a cylindrical coordinate system.

[4] On page 43.

[5] The exterior concentration is very suitable as the basis for the renormalization. Because the concentration only decreases further towards the interior of the particle and the natural lower limit is 0, by defining c_0 as the upper limit the dimensionless concentration is nicely bounded between 0 and 1.

From the definition of the coordinate transformation, we can replace the last term in the above equation to give

$$\frac{\partial}{\partial r} = \frac{\partial}{\partial \lambda}\frac{1}{R}. \tag{5.8}$$

Furthermore, from Equation 5.5, we find that

$$c = c_0\psi. \tag{5.9}$$

Insertion of Equations 5.8 and 5.9 into

$$D\frac{1}{r^2}\frac{\partial}{\partial r}\left(r^2\frac{\partial c}{\partial r}\right) = kc \tag{5.10}$$

yields

$$\frac{D}{\lambda^2}\frac{1}{R^2}\frac{\partial}{\partial \lambda}\left(\lambda^2\frac{\partial \psi c_0}{\partial \lambda}\right) = k\psi c_0 \tag{5.11}$$

which can be simplified to[6]

$$\frac{1}{\lambda^2}\frac{\partial}{\partial \lambda}\left(\lambda^2\frac{\partial \psi}{\partial \lambda}\right) = \frac{kR^2}{D}\psi. \tag{5.12}$$

We can identify a dimensionless term on the right-hand side of the equation which is known as the Thiele modulus as defined by[7]

$$\phi_1^2 = \frac{kR^2}{D}. \tag{5.13}$$

At first glance, it might seem convoluted to define the Thiele modulus as the square root of the right hand side term in Equation 5.12, but this relates back to the solution found for this equation, which is given by

$$\psi = \frac{1}{\lambda}\left(\frac{\sinh(\phi_1\lambda)}{\sinh(\phi_1)}\right). \tag{5.14}$$

> **Tip**
>
> A step-by-step derivation can be found on YouTube:
> https://youtu.be/9u-AUARVCZs.

At this point, let me also introduce the first derivative of this result, which is given by [8]

$$\psi' = \frac{1}{\sinh(\phi_1)}\left(\frac{\phi_1\cosh(\phi_1\lambda)}{\lambda} - \frac{\sinh(\phi_1\lambda)}{\lambda^2}\right). \tag{5.15}$$

Clearly, the Thiele modulus arises naturally from the non-dimensionalization procedure. Careful analysis of its terms shows that it displays the ratio between the reaction rate and the rate of diffusion. When the Thiele modulus is very large, the rate of reaction is much faster than the rate of diffusion and hence the porous particle suffers from internal mass

[6] Note that for a first-order reaction, the term c_0 cancels.

[7] Observe the subscript "1" for the Thiele modulus. It is sometimes used to indicate the order of the reaction. Different geometries and different reaction orders yield different Thiele moduli, so always keep an eye out for the details.

[8] This is relevant later on to establish molar fluxes through boundaries, necessary for calculating efficiency factors.

transport limitations. Conversely, when the Thiele modulus is very small, the rate of reaction is much slower than the rate of diffusion and the particle suffers from kinetic limitations. From a commercial perspective, operating a reactor in a mass-transport limiting situation is an utter waste of your expensive catalytic material.

Caution

The Thiele modulus arises from the non-dimensionalization of the model system. This non-dimensionalization is however not always possible and consequently a Thiele modulus cannot always be defined. A salient example is for a bimolecular reaction where there is no one-to-one correspondence between the concentration of the reactants. The Thiele modulus serves as a nice tool to approximate realistic systems using an idealized model system to obtain quick results, however as an engineer you should be conscious about its inherent limitations and know when to abandon the approach for a more accurate model description.

5.3 Finite volume model

The finite volume discretization of a spherical pellet is fairly straightforward. The largest difference with respect to the previous examples we have encountered lies in the geometry of the system and the corresponding coordinate system that is used to efficiently describe that geometry. Combining equations Equations 5.12 and 5.13 yields the following fundamental differential equation

$$\frac{1}{\lambda^2}\frac{\partial}{\partial\lambda}\left(\lambda^2\frac{\partial\psi}{\partial\lambda}\right) = \phi_1^2\psi, \tag{5.16}$$

with the following two boundary conditions

$$\psi|_{\lambda=1} = 1 \tag{5.17}$$

and

$$\nabla\psi|_{\lambda=0} = 0. \tag{5.18}$$

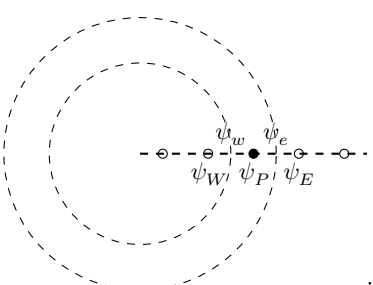

Figure 5.2: *Schematic depiction of the finite volume discretization of a spherical pellet. Note that the control volumes correspond to a series of concentric spherical shells whose volume is defined by their inner and outer radius.*

Application of the finite volume discretization procedure to Equation 5.16 gives the following integral formulation for a control volume

$$\iiint_V \frac{1}{\lambda^2}\frac{\partial}{\partial\lambda}\left(\lambda^2\frac{\partial\psi}{\partial\lambda}\right)\,dV = \iiint_V \phi_1^2\psi\,dV. \tag{5.19}$$

The control volumes of the spherical system correspond to concentric shells as schematically depicted in Figure 5.2. Note that the left-hand side of Equation 5.19 can be written as

$$\iiint_V \nabla \cdot \nabla\psi \, dV, \tag{5.20}$$

wherein it is critical to observe that $\nabla\psi$ constitutes a vector field. Thus, we are allowed to apply the divergence theorem (Equation 2.24) to rewrite the volume integral on the left hand side into a surface integral over the enclosing volume, yielding

$$\oiint_{S(V)} \nabla\psi \cdot \hat{n} \, dS = \iiint_V \phi_1^2 \psi \, dV. \tag{5.21}$$

which upon removal of those components in $\nabla\psi$ which are gradientless[9] gives

$$\oiint_{S(V)} \frac{\partial\psi}{\partial\lambda}\hat{n} \, dS = \iiint_V \phi_1^2 \psi \, dV, \tag{5.22}$$

where $\hat{n}$ effectively points radially outward, i.e. in the direction of $\hat{\rho}$.

Observe that the relatively complicated[10] Laplacian transforms to a much simpler equation corresponding to the *gradient* in spherical coordinates, as seen earlier in Equation 4.54.[11] Evaluating the integrals on both sides of the equation gives

$$(4\pi\lambda_e^2) \left.\frac{\partial\psi}{\partial\lambda}\right|_e - (4\pi\lambda_w^2) \left.\frac{\partial\psi}{\partial\lambda}\right|_w = \frac{4}{3}\pi\left(\lambda_e^3 - \lambda_w^3\right)\phi_1^2\psi, \tag{5.23}$$

wherein the terms $(4\pi\lambda_e^2)$ and $(4\pi\lambda_w^2)$ correspond to surface area of a sphere with radius λ_e and λ_w, respectively. Furthermore, the term $\frac{4}{3}\pi\left(\lambda_e^3 - \lambda_w^3\right)$ corresponds to a hollow spherical shell with outer and inner radius λ_e and λ_w, respectively.

Because there is no (direct) information on the boundaries of the control volumes, we have to approximate the values at these positions. To approximate the first derivative, we can utilize the known concentrations on the east and west control volumes.[12] A straightforward discretization technique is to take central point differences as given by

$$\left.\frac{\partial\psi}{\partial\lambda}\right|_e = \frac{\psi_E - \psi_P}{\Delta\lambda} \tag{5.24}$$

and

$$\left.\frac{\partial\psi}{\partial\lambda}\right|_w = \frac{\psi_P - \psi_W}{\Delta\lambda}. \tag{5.25}$$

Using this approximation, we arrive at the following equation[13]

$$\lambda_e^2\frac{\psi_E - \psi_P}{\Delta\lambda} - \lambda_w^2\frac{\psi_P - \psi_W}{\Delta\lambda} = \frac{1}{3}\left(\lambda_e^3 - \lambda_w^3\right)\phi_1^2\psi_P, \tag{5.26}$$

from which the finite volume coefficients for a central volume can be readily obtained. For the boundary cells, we have to carefully take the

[9] Recall from the problem definition that we assumed that there are no concentration gradients in the azimuthal and polar directions. Thus, these two components from the vector field $\nabla\psi$ vanish.

[10] At the least, more complicated than the Laplacian for a flat cartesian space.

[11] On page 43.

[12] Assuming they exist of course. For the control volumes at the particle boundaries, we have to apply some additional tricks.

[13] Also observe that I crossed out some common factors on both sides of the equation.

boundary conditions of the original differential equation into account when producing the finite volume coefficients. To start, consider the inner boundary at $\lambda = 0$. Because of spherical symmetry, the concentration on opposite sides with respect to the center of volume of the sphere should be equal and as a direct consequence of that, the first derivative of the concentration at $\lambda = 0$ should vanish. Taking this condition into account, we find the following equation for the innermost control volume

$$\lambda_e^2 \frac{\psi_E - \psi_P}{\Delta\lambda} = \frac{1}{3}\left(\lambda_e^3 - \lambda_w^3\right)\phi_1^2\psi_P \tag{5.27}$$

$$\lambda_e^2 \frac{\psi_E - \psi_P}{\Delta\lambda} = \frac{1}{3}\lambda_e^3\phi_1^2\psi_P, \tag{5.28}$$

wherein we observe that in comparison to Equation 5.26 the west term is simply absent. For the outermost control volume, the boundary conditions corresponds to a fixed concentration at $\lambda = 1$ which is defined as $\psi_{\lambda=1} = 1$. This puts us in a little bit of a conundrum. The concentration is only determined exactly at the boundary, but the approximation scheme for the eastside first derivative is defined with respect to a point that lies outside of the particle domain. As such, we have to introduce a discretization scheme that takes this subtle difference into account. Given the known concentrations ψ_e and ψ_P at the outer boundary, the first derivative of ψ at the boundary is approximated by[14]

$$\left.\frac{\partial\psi}{\partial\lambda}\right|_{\lambda=1} = \frac{1 - \psi_P}{\Delta\lambda/2}. \tag{5.29}$$

[14] Observe the two in the denominator on the right hand side of the equation. This difference is indeed quite subtle as neglecting to take the 2 into account does not yield a significantly worse representation. Careful numerical evaluation is however able to pick up on this so be a proper engineer and appropriately implement these nuances.

Implementation of the above approximation yields the following governing equation for the outermost control volume

$$\lambda_e^2 \frac{1 - \psi_P}{\Delta\lambda/2} - \lambda_w^2 \frac{\psi_P - \psi_W}{\Delta\lambda} = \frac{1}{3}\left(\lambda_e^3 - \lambda_w^3\right)\phi_1^2\psi_P, \tag{5.30}$$

An overview of the finite volume coefficients as extracted from Equations 5.26, 5.28 and 5.30 is found in Table 5.1.

Table 5.1: *Overview of the finite volume discretization constants for a spherical pellet with first order kinetics. Note that $\lambda_e = 1$ at $i = N - 1$.*

Terms	a_W	a_P	a_E	b
$i = 0$	0	$-\frac{\lambda_e^2}{\Delta\lambda} - \frac{\phi_1^2}{3}\left(\lambda_e^3 - \lambda_w^3\right)$	$\frac{\lambda_e^2}{\Delta\lambda}$	0
$0 < i < N-1$	$\frac{\lambda_w^2}{\Delta\lambda}$	$-\frac{\lambda_e^2}{\Delta\lambda} - \frac{\lambda_w^2}{\Delta\lambda} - \frac{\phi_1^2}{3}\left(\lambda_e^3 - \lambda_w^3\right)$	$\frac{\lambda_e^2}{\Delta\lambda}$	0
$i = N-1$	$\frac{\lambda_w^2}{\Delta\lambda}$	$-\frac{2\lambda_e^2}{\Delta\lambda} - \frac{\lambda_w^2}{\Delta\lambda} - \frac{\phi_1^2}{3}\left(\lambda_e^3 - \lambda_w^3\right)$	0	$-\frac{2\lambda_e^2}{\Delta\lambda}$

In Figure 5.3, the result of the numerical model is compared against the analytical solution as given in Equation 5.14. From the figure, it can be

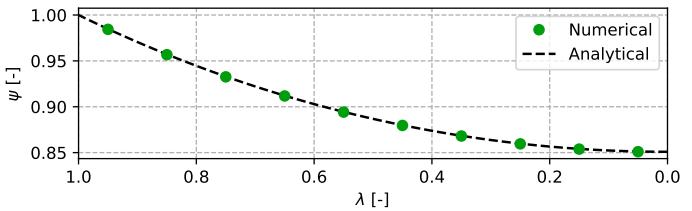

Figure 5.3: *Dimensionless concentration profile for a spherical pellet with* $\phi_1 = 1$.

seen that the numerical model is in excellent agreement with the analytical result.

Similar to the results as found in Section 2.3, the discretization scheme as shown in Table 5.1 is, generally speaking, accurate up to second order. An analysis of the MAPE as function of the spatial step size, for three different values of ϕ, is shown in Figure 5.4. We observe that the order of the method and furthermore the error metric is strongly dependent on the value of the Thiele modulus. As such, depending on the Thiele modulus, significantly more control volumes are required to get an accurate description.

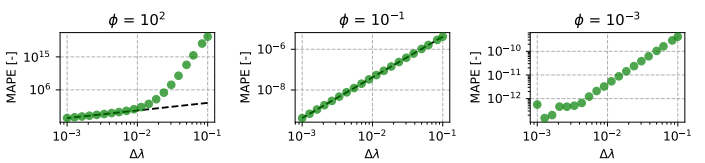

Figure 5.4: *Error analysis of the finite volume model as function of the Thiele modulus. For large number of control volumes, an order* $\mathcal{O}$ *is found for* $\phi > 0.1$. *For very small* ϕ, *the error is very small and the order of the method cannot be established by means of simple linear fitting.*

Indeed, from Figure 5.4 it becomes clear that for large values of ϕ, a large number of control volumes is necessary if we want the errors to be much smaller than the actual values. For example, when $\phi = 100$ and $\Delta\lambda < 0.01$, i.e. for more than 100 control volumes, the order of the method is $\mathcal{O} \approx 2$ and MAPE is relatively small. However for fewer than 100 control volumes, the MAPE rapidly increases to unacceptable values. For $\phi = 0.1$, we observe that the method produces accurate results using as few as 10 control volumes. For very small ϕ values, i.e. $\phi \ll 10^{-3}$, the MAPE is observed to be very small, irrespective of the number of control volumes used.

This rather strong dependency of the accuracy of the method on the value for ϕ can be easily explained by considering the concentration profiles as function of ϕ as shown in Figure 5.5. When ϕ is very large, there is a sudden and rapid decrease in the concentration as function of

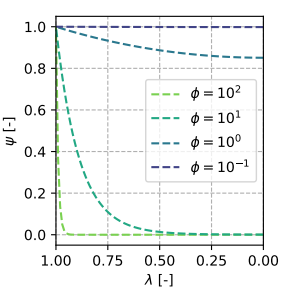

Figure 5.5: *Concentration profile as function of* ϕ.

λ. To accurately represent that steep drop in concentration, many control volumes for that region of λ are required. For smaller values of ϕ, this decrease in concentration is much more steadily and for the smallest values of ϕ, the concentration profile is in fact rather uniform throughout the particle. For these latter two situations, only a relatively few number of control volumes would be necessary to obtain an accurate representation.

5.4 Temperature effects

Having established a working numerical model and observed that it is in excellent agreement with the analytical result, we can introduce a nice *in silico* experiment wherein we vary the Thiele modulus as a function of temperature. Consider the reaction rate constant k as part of the Thiele modulus. This reaction rate constant is defined for a particular temperature, let us define this reference temperature as T_{ref}. Furthermore, let us assume that from detailed kinetic tests[15] the apparent activation energy has been established. With these kinetic factors established, we can express the rate constant at a different temperature T_c with respect to the conditions known for the reference temperature by means of

[15] Or if you want to stick to in silico experiments, assume that high quality quantum chemical simulations in conjunction with microkinetic modeling has been conducted.

$$k\left(T\right) = k\left(T = T_{\text{ref}}\right) \exp\left(-\frac{\Delta E_{\text{act}}}{R}\left(\frac{1}{T_c} - \frac{1}{T_{\text{ref}}}\right)\right), \tag{5.31}$$

wherein R is the gas phase constant. From the above equation, we extract a temperature dependent scaling coefficient ν as given by

$$\nu = \exp\left(-\frac{\Delta E_{\text{act}}}{R}\left(\frac{1}{T_c} - \frac{1}{T_{\text{ref}}}\right)\right). \tag{5.32}$$

which describes how the Thiele modulus will change as function of temperature, which is given by

$$\phi_1(T) = \sqrt{\nu}\phi_1(T = T_{\text{ref}}). \tag{5.33}$$

Let us now investigate how the Thiele modulus and its corresponding dimensionless concentration profile changes as function of temperature. For this *in silico* experiment, we have taken a reference temperature of $T = 400$ K and explore the profile between $300\text{ K} < T < 500\text{ K}$. The apparent activation energy has been set to $\Delta E_{\text{act}} = 100$ kJ/mol.[16] In Figure 5.6, the result of this analysis is shown.

[16] This value is in the right ballpark for a typical catalytic reaction.

From Figure 5.6, it can be readily seen that at very low temperature, the dimensionless concentration profile is rather flat and very close to unity. At this low temperature, the reaction rate is very slow and diffusion is much faster than reaction. As a consequence, the reactant diffuses relatively rapidly into the porous catalyst pellet without being consumed in the reaction. Conversely, at high temperature, we observe that the dimensionless concentration profile is rapidly decreasing towards zero.

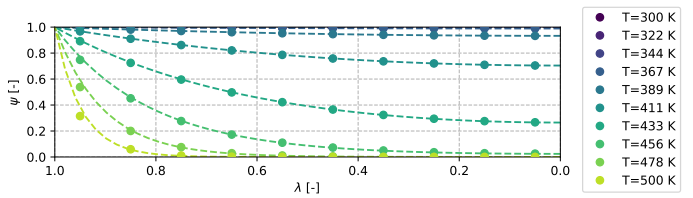

Figure 5.6: *Dimensionless concentration profile as function of temperature for a spherical pellet with* $\phi_1\left(T_{ref}\right) = 1$.

In that situation, the rate of diffusion cannot keep up with the rate of reaction and as such, a depletion zone inside the catalyst pellet is observed. Such a situation is of course quite unideal as part of the catalyst pellet remains underutilized.

5.5 Efficiency factor and temperature effects

In Figure 5.6, it can be seen that as function of temperature, there are vastly different concentration profiles in the spherical pellet. A rather straightforward way to characterize these profiles is to introduce the concept of an efficiency factor. This efficiency factor is defined such that we compare the rate of chemical conversion inside the catalyst pellet with the optimal theoretical rate under the condition that the concentration of the reactant throughout the particle is identical to the bulk concentration outside the particle. Assuming fully isothermal operation, the efficiency factor always lies between 0 and 1.[17]

[17] Under non-isothermal operation, the efficiency factor can exceed 1. This happens when the reaction is exothermic and due to build-up of heat, the rate of chemical conversion inside the particle increases.

The optimal rate of chemical conversion $\dot{M}_{\text{opt}}$ for the particle as a whole is given by

$$\dot{M}_{\text{opt}} = \frac{4}{3}\pi R^3 k c_0 \tag{5.34}$$

The actual rate of conversion corresponds to the following integral

$$\dot{M} = \iiint_V k c(r) dV \tag{5.35}$$

which at steady state corresponds to the total flux via diffusion over the boundary of the particle

$$\dot{M} = D \oiint_{S(V)} \frac{\partial c}{\partial r} \psi' \hat{n} dS \tag{5.36}$$

$$= 4\pi D R^2 \left.\frac{\partial c}{\partial r}\right|_{r=R} \tag{5.37}$$

$$= 4\pi D R c_0 \frac{\partial \psi}{\partial \lambda}. \tag{5.38}$$

The efficiency factor η can now be established by combining Equations 5.34 and 5.38, which gives

$$\eta = \frac{\dot{M}}{\dot{M}_{\text{opt}}} = \frac{4\pi D R c_0}{\frac{4}{3}\pi R^3 k c_0} \left.\frac{\partial \psi}{\partial \lambda}\right|_{\lambda=1} \tag{5.39}$$

$$= \frac{3D}{R^2 k} \left.\frac{\partial \psi}{\partial \lambda}\right|_{\lambda=1} \tag{5.40}$$

$$= \frac{3}{\phi_1^2} \left.\frac{\partial \psi}{\partial \lambda}\right|_{\lambda=1} \tag{5.41}$$

Inserting Equation 5.15 in Equation 5.41 yields

$$\eta = \frac{3}{\phi_1^2} \left.\frac{\partial \psi}{\partial \lambda}\right|_{\lambda=1} \tag{5.42}$$

$$= \frac{3}{\phi_1^2 \sinh(\phi_1)} \left(\frac{\phi_1 \cosh(\phi_1 \lambda)}{\lambda} - \frac{\sinh(\phi_1 \lambda)}{\lambda^2} \right) \Bigg|_{\lambda=1} \tag{5.43}$$

$$= \frac{3}{\phi_1^2} \left(\frac{\phi_1 \cosh(\phi_1) - \sinh(\phi_1)}{\sinh(\phi_1)} \right) \tag{5.44}$$

$$= \frac{3}{\phi_1^2} \left(\phi_1 \coth(\phi_1) - 1 \right). \tag{5.45}$$

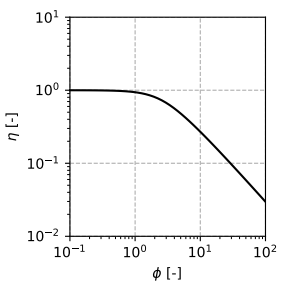

Figure 5.7: *Efficiency factor η as function of the Thiele modulus ϕ for a spherical pellet with first order kinetics.*

In Figure 5.7, the relationship between η and ϕ is depicted. From this figure, we can observe that in the limit $\phi_1 \to 0$, $\eta \to 1$ and in the limit $\phi_1 \to \infty$, $\eta \to 0$. We can derive the lower limit ($\phi_1 \to 0$) by considering the power (Laurent) series expansion of $\coth(\phi_1)$

$$\coth(\phi_1) = \frac{1}{\phi_1} + \frac{\phi_1}{3} - \frac{\phi_1^3}{45} + \frac{2\phi_5}{945} - \cdots. \tag{5.46}$$

Inserting the Laurent series into Equation 5.45 and taking the limit $\phi_1 \to 0$, yields

$$\lim_{\phi_1 \to 0}(\eta) = \lim_{\phi_1 \to 0} \left(\frac{3}{\phi_1^2} \left(\phi_1 \coth(\phi_1) - 1 \right) \right) \tag{5.47}$$

$$= \lim_{\phi_1 \to 0} \left(\frac{3}{\phi_1^2} \left(\phi_1 \left(\frac{1}{\phi_1} + \frac{\phi_1}{3} - \frac{\phi_1^3}{45} + \frac{2\phi_1^5}{945} + \cdots \right) - 1 \right) \right) \tag{5.48}$$

$$= \lim_{\phi_1 \to 0} \left(\frac{3}{\phi_1^2} \left(\frac{\phi_1^2}{3} - \frac{\phi_1^4}{45} + \frac{2\phi_1^6}{945} + \cdots \right) \right) \tag{5.49}$$

$$= \lim_{\phi_1 \to 0} \left(\frac{3}{\phi_1^2} \frac{\phi_1^2}{3} \right) = 1. \tag{5.50}$$

wherein we have set the higher order in Equation 5.49, i.e. the terms in ϕ^4 and higher, to 0.

For $\phi_1 \to \infty$, $\coth \phi_1$ tends to converge to unity. As such, in the situation of very large Thiele moduli ϕ_1, Equation 5.45 can be simplified to

$$\eta \approx \frac{3}{\phi_1^2}\left(\phi_1 - 1\right), \text{ for } \phi_1 \gg 30 \tag{5.51}$$

$$\approx \frac{3}{\phi_1^2}\left(\phi_1\right) \tag{5.52}$$

$$= \frac{3}{\phi_1}. \tag{5.53}$$

By critical analysis of Figure 5.7, it can indeed be observed that the slope on the right hand side corresponds to a value of -1.[18]

[18] Note that Figure 5.7 is a logarithmic plot, so the slope corresponds to $\frac{\partial \ln \eta}{\partial \ln \phi}$, which for Equation 5.53 yields -1.

Since the Thiele modulus depends on the temperature, we can explore the efficiency factor as function of temperature by combining Equations 5.32, 5.33 and 5.45. Considering a reference temperature of $T = 400$K at which $\phi_1 = 1$, we obtain for various values for the apparent activation energy the result as shown in Figure 5.8.

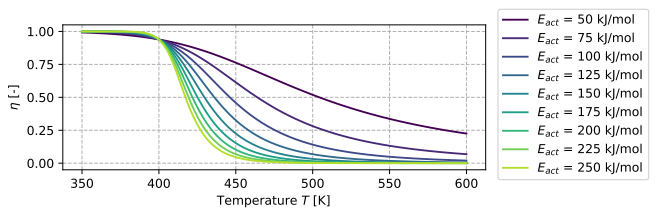

Figure 5.8: *Efficiency factor as function of temperature for different values of the apparent activation energy.*

From Figure 5.8, we observe a sigmoidal type of curve as function of temperature. In the low temperature regime, the reaction is kinetically limited and as such, the efficiency factor is very close to unity. With increasing temperature, the efficiency decreases and in the high temperature regime, the reaction is limited by the rate of mass-transport. This gives an efficiency factor of nearly zero.

Furthermore, Figure 5.8 allows us to investigate the effect of the apparent activation energy on the curves. When the apparent activation energy is high, the reaction rate is strongly affected by changes in temperature and a rather steep decrease in the efficiency factor as function of temperature is observed. Alternatively, if the apparent activation energy is low, the reaction rate is relatively unaffected by changes in temperature and this is reflected by an almost linear response of the efficiency factor with respect to temperature.

An important consequence of this is that when one is performing kinetic analysis of a catalytic reaction, one has to ensure that the reactor is operated in a kinetically limited regime. If this is not the case, then all measurements will be muddled by mass-transport limitations. To

get a better understanding of this, let us aim to construct an analytical expression for the apparent activation energy as function of temperature.

From the problem formulation, it can be stated that the volumetric reaction rate is given by

$$r = \phi_1^2 \cdot \eta, \tag{5.54}$$

wherein η is given by Equation 5.45 and its dependency on the temperature is given by Equations 5.32 and 5.33. From the volumetric reaction rate r, the apparent activation energy can be established via

$$\Delta E_{\text{act}}^{\text{app}} = RT^2 \frac{\partial \ln r^+}{\partial T} \tag{5.55}$$

Despite that Equations 5.32, 5.33 and 5.45 are relatively complicated functions, they are all well-behaved and sufficiently smooth by which the differential as given by Equation 5.55 exists. The result is[19]

$$\Delta E_{\text{act}}^{\text{app}} = \Delta E_{\text{act}} {\phi_1}' \frac{\sqrt{\nu}\coth\left(\sqrt{\nu}{\phi_1}'\right) - \nu\,\text{csch}\left(\sqrt{\nu}{\phi_1}'\right)}{2\sqrt{\nu}{\phi_1}'\coth\left(\nu{\phi_1}'\right) - 2}, \tag{5.56}$$

wherein ν is given by Equation 5.32, csch is the hyperbolic cosecant and ${\phi_1}'$ is the Thiele modulus at $T = T_{\text{ref}}$. Without any loss of generality, we can define ${\phi_1}' = 1$, by which Equation 5.56 can be simplified to

$$\Delta E_{\text{act}}^{\text{app}} = \Delta E_{\text{act}} \frac{\sqrt{\nu}\coth\left(\sqrt{\nu}\right) - \nu\,\text{csch}\left(\sqrt{\nu}\right)}{2\sqrt{\nu}\coth\left(\nu\right) - 2}. \tag{5.57}$$

From Equation 5.57 we can extract a modulation factor ζ which describes how the actual apparent activation energy changes due to internal mass-transport as function of temperature. This modulation factor is given by

$$\zeta = \frac{\Delta E_{\text{act}}^{\text{app}}}{\Delta E_{\text{act}}} \tag{5.58}$$

$$= \frac{\sqrt{\nu}\coth\left(\sqrt{\nu}\right) - \nu\,\text{csch}\left(\sqrt{\nu}\right)}{2\sqrt{\nu}\coth\left(\nu\right) - 2}. \tag{5.59}$$

An interesting thought experiment is to explore the value of ζ in the limits $T \to 0$ and $T \to \infty$ as these two limiting conditions correspond to a fully kinetically limited regime and a fully mass-transport limiting regime. These limits are however certainly nontrivial to establish and require a few mathematical tricks to do so.[20] They are as follows

$$\lim_{T\to 0}\left(\frac{\sqrt{\nu}\coth\left(\sqrt{\nu}\right) - \nu\,\text{csch}\left(\sqrt{\nu}\right)}{2\sqrt{\nu}\coth\left(\nu\right) - 2}\right) = 1 \tag{5.60}$$

and

$$\lim_{T\to \infty}\left(\frac{\sqrt{\nu}\coth\left(\sqrt{\nu}\right) - \nu\,\text{csch}\left(\sqrt{\nu}\right)}{2\sqrt{\nu}\coth\left(\nu\right) - 2}\right) = \frac{1}{2}. \tag{5.61}$$

[19] The result does not look pretty, but we should be happy that an analytical solution exists in the first place. If you feel courageous, you can try to reproduce this result, but only do so when the weather is very bad. If that is not the case, just enjoy life.

[20] Especially the limit $T \to 0$ is difficult. So let me do that for you. And trust me on the results, I am an engineer.

In conclusion, under strong internal mass-transport limitations, the measured apparent activation energy will be **half** the value of the true kinetic apparent activation energy. In Figure 5.9, a comparison is made between the efficiency factor η and the modulation factor ζ as function of temperature. Clearly, the two curves are related to each other and it can be seen that when the efficiency factor approaches zero, the modulation factor approaches a half.

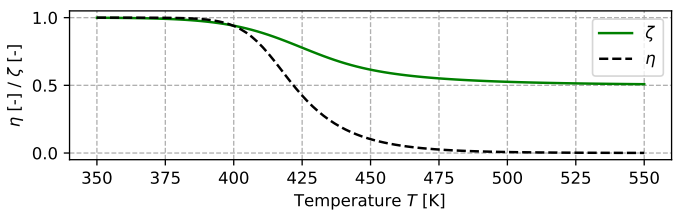

Figure 5.9: *Efficiency factor η and modulation factor ζ as function of temperature.*

It is interesting to note that Weisz and Prater [4] come to the same result, but their reasoning is based on a much more general approach of the problem and does not yield the full detail of the form as presented in Equation 5.59.[21] They start out by noting that the measured apparent activation energy is given by

$$\Delta E_{\text{act}}^{\text{app}} = RT^2 \frac{\partial \ln R}{\partial T} \tag{5.62}$$

$$= RT^2 \frac{\partial \ln (k\eta)}{\partial T} \tag{5.63}$$

$$= RT^2 \left(\frac{\partial \ln k}{\partial T} + \frac{\partial \ln \eta}{\partial T} \right) \tag{5.64}$$

$$= \Delta E_{\text{act}}^{\text{true}} + RT^2 \frac{\partial \ln \eta}{\partial T} \tag{5.65}$$

Since[22]

$$\frac{\partial \ln \eta}{\partial T} = \frac{\partial \ln \eta}{\partial \ln \phi} \cdot \frac{\partial \ln \phi}{\partial T} \tag{5.66}$$

and

$$\frac{\partial \ln \phi}{\partial T} = \frac{\partial}{\partial T} \ln \left(\sqrt{\frac{kR^2}{D}} \right) \tag{5.67}$$

$$= \frac{\partial}{\partial T} \ln \left(\sqrt{\frac{R^2}{D} \cdot \nu \exp \left(-\frac{\Delta E_{\text{act}}^{\text{true}}}{RT} \right)} \right) \tag{5.68}$$

$$= \frac{1}{2} \frac{\Delta E_{\text{act}}^{\text{true}}}{RT^2} \tag{5.69}$$

it follows that

[21] Note that Equation 5.59 is rather specific for the problem at hand and only valid for spherical pellets with first-order kinetics.

[22] Since the derivation of Weisz and Prater is in more general terms, I will drop the subscript "1" from ϕ and introduce it later on when the details become specific once again.

$$\Delta E_{act}^{app} = \Delta E_{act}^{true} + \frac{1}{2}\Delta E_{act}^{true}\frac{\partial \ln \eta}{\partial \ln \phi} \tag{5.70}$$

which can be simplified to[23]

$$\frac{\Delta E_{act}^{app}}{\Delta E_{act}^{true}} = 1 + \frac{1}{2}\frac{\partial \ln \eta}{\partial \ln \phi}. \tag{5.71}$$

Since η is known[24] from Equation 5.45, we can readily determine the derivative $\frac{\partial \ln \eta}{\partial \ln \phi_1}$ to be

$$\frac{\partial \ln \eta}{\partial \ln \phi_1} = \frac{2 - \phi_1\left(\coth \phi_1 + \phi_1 \operatorname{csch}^2 \phi_1\right)}{\phi_1 \coth \phi_1 - 1}. \tag{5.72}$$

In this formulation, instead of exploring the limits as function of temperature, we can explore the limits as function of the Thiele modulus. In the limit of a very small Thiele modulus, it is found that

$$\lim_{\phi_1 \to 0} \left(\phi_1 \coth \phi_1\right) = 1 \tag{5.73}$$

and

$$\lim_{\phi_1 \to 0} \left(\phi_1^2 \operatorname{csch}^2 \phi_1\right) = 1, \tag{5.74}$$

by which we find that

$$\lim_{\phi_1 \to 0} \left(\frac{2 - \phi_1\left(\coth \phi_1 + \phi_1 \operatorname{csch}^2 \phi_1\right)}{\phi_1 \coth \phi_1 - 1} \right) = 0. \tag{5.75}$$

Furthermore, since

$$\lim_{\phi_1 \to \infty} \left(\phi_1 \coth \phi_1\right) \to \infty \tag{5.76}$$

and

$$\lim_{\phi_1 \to \infty} \left(\phi_1^2 \operatorname{csch}^2 \phi_1\right) = 1, \tag{5.77}$$

we find that

$$\lim_{\phi_1 \to \infty} \left(\frac{2 - \phi_1\left(\coth \phi_1 + \phi_1 \operatorname{csch}^2 \phi_1\right)}{\phi_1 \coth \phi_1 - 1} \right) = -1. \tag{5.78}$$

From these limits, we can establish that for very small values of the Thiele modulus (small diffusion resistance), the apparent and true activation energies are the same while for very large Thiele moduli (large diffusion resistance), the ratio between apparent and true activation energies yields a half.

[23] I need to emphasize here that in the original work of Weisz and Prater, there is mistake wherein the two terms in the derivative on the right hand side of the equation are swapped. Caveat lector!

[24] As a kind reminder, this function is only valid for spherical pellets and first order kinetics.

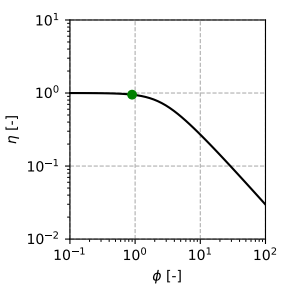

Figure 5.10: *Efficiency factor η as function of the Thiele modulus ϕ for a spherical pellet with first order kinetics. The point at which the Weisz-Prater crition is met is indicated by a green circle.*

5.6 Weisz-Prater criterion

The work of Weisz and Prater was one of the first wherein a criterion was established, later on named after them, that defines appropriate working conditions under which kinetic measurements should be executed. In their original work, they simply state that the efficiency factor η should always be above 95% and an appropriate Thiele modulus ϕ should be found that meets this constraint. To come to such a value, we have to resort to using numerical approximation wherein we find a value of ϕ according to the following transcendental equation

$$\frac{3}{\phi_1^2}\left(\phi_1 \coth\left(\phi_1\right) - 1\right) = 0.95. \tag{5.79}$$

This equation yields a single solution for $\phi = 0.898586879142$. In Figure 5.10, the position of this point is visualized. For all values of $\phi < 0.898586879142$, the efficiency factor η will be larger than 95% and these correspond to suitable conditions to conduct kinetic measurements.

Later on, their procedure was formalized in the definition of the Weisz-Prater parameter

$$C_{\mathrm{WP}} = \eta \cdot \phi_1^2 = 3\left(\phi_1 \coth \phi_1 - 1\right). \tag{5.80}$$

Considering the term $\eta \cdot \phi_1^2$, the Weisz-Prater parameter is rather intuitive to understand. Since η is the ratio between the observed reaction rate and the reaction rate evaluated at the boundary of the catalyst pellet and ϕ^2 the ratio between the reaction rate evaluated at the boundary of particle and the rate of diffusion, the product of these two is thus the ratio between the observed rate of reaction and the rate of diffusion.

As such, if $C_{\mathrm{WP}} \ll 1$, it is clear that the rate of reaction is much smaller than the rate of diffusion and we anticipate no concentration gradient inside the particle. On the other hands, if $C_{\mathrm{WP}} \gg 1$, the reaction is severely restricted by internal diffusion limitations and a very steep concentration gradient inside the particle is to be expected.

The actual value for C_{WP} can be established via both experimental as well as theoretical means. Either one explicitly measures the actual volumetric[25] reaction rate r or computes it by means of a numerical model. With this value established and using known values for the diffusion and the particle size, the Weisz-Prater parameter C_{WP} can be evaluated by means of

$$C_{\mathrm{WP}} = \frac{rR^2}{Dc_0}. \tag{5.81}$$

[25] I need to emphasize here that the volumetric reaction rate is here defined as per volume of the catalyst pellet.

5.7 Exercises

Exercise 5.1

a) Construct a FVM model for a spherical pellet for an arbitrary n-th order reaction ($n \in \mathbb{Z}_{\geq 1}$) where the concentration profile is given by the following differential equation (using dimensionless numbers)

$$\frac{1}{\lambda^2}\frac{d}{d\lambda}\left(\lambda^2 \frac{d\psi}{d\lambda}\right) = \phi_n^2 \psi^n \tag{5.82}$$

In the above equation, ϕ_n corresponds to the Thiele modulus for a spherical system and a n-th order reaction. When $n = 1$, the above differential equation can be discretized into a linear system of algebraic equations $\mathbf{A}\vec{\psi} = \vec{b}$. However for any $n > 1$, this is no longer possible and one has move the reaction terms to the solution vector $\vec{b}$ such that $\vec{b}$ **explicitly** depends on $\vec{\psi}$ such that

$$\vec{b} = f(\vec{\psi}). \tag{5.83}$$

Construct expressions for the coefficients A_{ij} and b_i and show that

$$b_i = \frac{\lambda_e^3 - \lambda_w^3}{3}\phi_n^2 \psi_i^n \;\forall\; i \in (0, N-2) \tag{5.84}$$

which correspond to reaction terms.

b) The above system cannot be solved using a linear solver like `np.linalg.solve`, but one is able to solve this system in an iterative fashion. Take $n = 1$ and $\phi_1 = 1$ and show that the concentration profile converges to the analytical solution using the following recursive relation (this procedure is colloquially known as a '*hammer and anvil*' method)

$$\vec{\psi}^{(i+1)} = \mathbf{A}^{-1}\vec{b}(\vec{\psi}^{(i)}), \tag{5.85}$$

where $\vec{\psi}^{(i+1)}$ corresponds to the dimensionless concentration profile at iteration $i+1$ and $\mathbf{A}^{-1}$ is the matrix inverse of $\mathbf{A}$. Start with an initial concentration profile of $\psi = 1$, irrespective of the position λ. Use $N = 20$ control volumes. Assume the system is converged when

$$\sum_j \left(\psi_j^{(i+1)} - \psi_j^{(i)}\right)^2 < 10^{-5}. \tag{5.86}$$

How many iterations are needed to achieve convergence?

c) Repeat the procedure of the previous subquestion, but now for $n = 2$.

d) Increase the Thiele modulus to $\phi = 5$. If you now try the iterative procedure you will observe you run into numerical problems. The reason is that the iterative procedure tends to overshoot, resulting negative concentrations, entering a domain outside of the allowed configuration space of valid solutions. To prevent this, one can slowly mix in the new solution into the old one, via a process called linear mixing. For this procedure, a linear mixing constant $\alpha \in (0, 1)$ is introduced such that

$$\vec{\psi}^{(i+1)} = \alpha \cdot \left(\mathbf{A}^{-1} \vec{b}(\vec{\psi}^{(i)}) \right) + (1 - \alpha) \vec{\psi}^{(i)}. \tag{5.87}$$

Use a value of $\alpha = 0.1$ and show that the numerical procedure is stable. Compare the concentration profiles for $n = 1$ and $n = 2$ using $\phi = 5$. Rationalize the result.

.

6 | NON-ISOTHERMAL CATALYST PARTICLES

Contents

6.1 Introduction

In the previous chapter, the concentration inside a catalyst pellet was explored as function of the Thiele modulus. Herein, we observed that the value for the Thiele modulus strongly depends on the temperature of the system. This analysis was conducted in the limit of isothermal operation, i.e. assuming that the transport of heat throughout the catalyst pellet is very efficient. When this is not the case, we have to evaluate the non-isothermal scenario which is the topic of this chapter.

6.2 Coupling of differential equations

To describe the thermal effects inside the spherical catalyst particle, in addition to the mole balance, the following energy balance is introduced[1]

$$\kappa \nabla^2 T = \Delta H_r k c, \tag{6.1}$$

wherein κ is the thermal conductivity and ΔH_r the heat of the reaction. The mass balance remains the same same and is given by

$$D \nabla^2 c = k c. \tag{6.2}$$

We now divide Equation 6.1 by κ and multiply Equation 6.2 by $\frac{\Delta H_r}{\kappa}$ by which we obtain

$$\nabla^2 T = \frac{\Delta H_r}{\kappa} k c, \tag{6.3}$$

and

[1] Note that ΔH_r is negative for an exothermic reaction and k is per definition positive, hence for an exothermic reaction this equation correctly predicts an increase in temperature.

$$\frac{D\Delta H_r}{\kappa}\nabla^2 c = \frac{\Delta H_r}{\kappa}kc. \tag{6.4}$$

Let us introduce the auxiliary variable α as given by

$$\alpha = \frac{\Delta H_r D}{\kappa}, \tag{6.5}$$

by which we can rewrite Equation 6.4 as

$$\alpha\nabla^2 c = \frac{\Delta H_r}{\kappa}kc. \tag{6.6}$$

Because α is a simple scalar, Equations 6.3 and 6.6 have the same source/sink term. This means that the difference f as given by

$$\alpha c = T + f \tag{6.7}$$

should satisfy the Laplace equation

$$\nabla^2 f = 0. \tag{6.8}$$

Since we assume that the concentration and temperature at the outer edge of the catalyst particle is fixed and given by c_0 and T_0 respectively, we obtain the following identity

$$\alpha c_0 = T_0 + f_0, \tag{6.9}$$

wherein f_0 is a constant. Any function f that satisfies the Laplace equation, i.e. Equation 6.8, and is constant at the enclosing boundaries of a volume is constant throughout that volume.[2] As such, this implies that f_0 is constant throughout the catalyst particle by which we have identified a one-to-one association between the concentration and the temperature in the catalyst particle as given by

$$\alpha c = T + f_0. \tag{6.10}$$

Combining Equations 6.9 and 6.10 and using the definition of α as given by Equation 6.5, it follows that

$$(T - T_0) = \frac{\Delta H_r D}{\kappa}(c - c_0). \tag{6.11}$$

or since the concentration c decreases throughout the course of the reaction, it is more intuitive to write[3]

$$(T - T_0) = \frac{(-\Delta H_r)\, D}{\kappa}(c_0 - c) \tag{6.12}$$

$$\Delta T = -\alpha(c_0 - c) \tag{6.13}$$

Due to this one-to-one association, we are only required to solve either one of the differential equations Equations 6.1 and 6.2 and can obtain via the relation in Equation 6.12 the profile of the other variable.

[2] This is a mathematical way of saying that if there is nothing inside a volume that can produce or consume a substance, i.e. there are no source or sink terms, and if the value of that substance is fixed at the boundaries of an enclosed domain, then the value for that substance should be uniform and constant throughout that domain.

[3] It can readily verified that for an exothermic reaction that temperature and concentration are negatively correlated. As such, a decrease in the concentration corresponds to an increase in temperature.

Before proceeding towards the numerical implementation, it is advantageous to nondimensionalize the equations. To start, let us explicitly define the effect of temperature in Equation 6.2. Given a rate constant k at arbitrary temperature T with respect to the rate constant k_0 at some fixed reference temperature T_0, we can state that

$$\frac{k}{k_0} = \frac{\nu \exp\left(-\frac{\Delta E_{\text{act}}}{RT}\right)}{\nu \exp\left(-\frac{\Delta E_{\text{act}}}{RT_0}\right)} \tag{6.14}$$

from which it can be found that

$$k = k_0 \frac{\nu \exp\left(-\frac{\Delta E_{\text{act}}}{RT}\right)}{\nu \exp\left(-\frac{\Delta E_{\text{act}}}{RT_0}\right)} \tag{6.15}$$

$$= k_0 \exp\left(-\frac{\Delta E_{\text{act}}}{R}\left(\frac{1}{T} - \frac{1}{T_0}\right)\right). \tag{6.16}$$

Since

$$T = T_0 + \Delta T \tag{6.17}$$

and inserting this expression into Equation 6.16, we can find that

$$k = k_0 \exp\left(-\frac{\Delta E_{\text{act}}}{R}\left(\frac{1}{T_0 + \Delta T} - \frac{1}{T_0}\right)\right) \tag{6.18}$$

$$= k_0 \exp\left(-\frac{\Delta E_{\text{act}}}{R}\left(\frac{T_0}{T_0\left(T_0 + \Delta T\right)} - \frac{\left(T_0 + \Delta T\right)}{T_0\left(T_0 + \Delta T\right)}\right)\right) \tag{6.19}$$

$$= k_0 \exp\left(-\frac{\Delta E_{\text{act}}}{R}\left(\frac{1}{T_0}\frac{-\Delta T}{\left(T_0 + \Delta T\right)}\right)\right) \tag{6.20}$$

$$= k_0 \exp\left(-\frac{\Delta E_{\text{act}}}{R}\left(-\frac{1}{T_0}\frac{\Delta T}{T_0}\frac{1}{1 + \Delta T/T_0}\right)\right) \tag{6.21}$$

$$= k_0 \exp\left(\frac{\Delta E_{\text{act}}}{RT_0}\left(\frac{\Delta T}{T_0}\frac{1}{1 + \Delta T/T_0}\right)\right). \tag{6.22}$$

Via this gross spectacle of mathematical juggling[4] we can readily establish two new dimensionless numbers, i.e. the dimensionless maximum temperature difference β as given by

$$\beta = \left(\frac{\Delta T}{T_0}\right)_{\text{max}} = \frac{c_0 \Delta H_r D}{\kappa T_0}. \tag{6.23}$$

and the dimensionless Arrhenius number γ as defined by

$$\gamma = \frac{\Delta E_{\text{act}}}{RT_0}. \tag{6.24}$$

Application of Equation 5.5 to Equation 6.13 yields

$$\Delta T = -\alpha c_0 \left(1 - \psi\right) \tag{6.25}$$

[4] It might look like a random collection of operations, but I am in fact shuffling the terms such that I obtain a set of terms that are dimensionless. For example, note that every T is divided by T_0.

and thus

$$\frac{\Delta T}{T_0} = -\frac{\alpha}{T_0} c_0 \left(1 - \psi\right) \tag{6.26}$$

$$= \beta(1 - \psi) \tag{6.27}$$

which together with Equation 6.22 and Equation 5.6, we can use to rewrite Equation 6.2 as

$$D\nabla_r^2 c = k_0 \exp\left(\frac{\Delta E_{\text{act}}}{RT_0}\left(\frac{\Delta T}{T_0}\frac{1}{1 + \Delta T/T_0}\right)\right) c \tag{6.28}$$

$$\nabla_\lambda^2 \psi = \frac{k_0 R^2}{D} \exp\left(\gamma \frac{\beta(1-\psi)}{1 + \beta(1-\psi)}\right) \psi \tag{6.29}$$

$$\nabla_\lambda^2 \psi = \phi_1^2 \psi \exp\left(\beta\gamma \frac{(1-\psi)}{1 + \beta(1-\psi)}\right) \tag{6.30}$$

wherein we have used the previously established definition for a Thiele modulus as given in Equation 5.13 and use the notation ∇_r^2 and ∇_λ^2 to differentiate whether the Laplacian operator is with respect to the radius r of the dimensionless radius λ.[5]

[5] Note that from here on, I am going to drop this subscript λ. It only serves to explicitly show the unit transformation.

Equation 6.30 is associated with two boundary conditions, i.e. a Dirichlet boundary condition at the particle edge

$$\psi|_{\lambda=1} = 1 \tag{6.31}$$

and a Neumann boundary condition at the particle center

$$\nabla\psi|_{\lambda=0} = 0, \tag{6.32}$$

both identical to the boundary conditions as shown previously in Equation 5.17 and Equation 5.18.

6.3 Shooting method

Because of the right-hand side term in Equation 6.30, a finite volume discretization of this ordinary differential equation gives non-linear terms in the vector $\vec{b}$.[6] As such, we can no longer use simple matrix-vector algebra to solve this kind of problem. To compound to the complexity, due to the exponential term in the right hand side which explicitly depends on the concentration ψ, the problem is considered to be very stiff[7] and specialized numerical integration routines are required to solve this problem. The procedure to tackle Equation 6.30 is known as a "shooting" method[5] and we here explain upon the methodology as published in the seminal paper of Weisz and Hicks.[6]

[6] See Equation 2.38 on page 19.

[7] Stiffness is mathematically rather poorly defined, but basically it means that certain numerical methods for solving stiff equations are unstable unless the step size is taken to be extremely small.

Instead of solving the boundary value problem as given by Equation 6.30 with the boundary conditions Equations 6.31 and 6.32, a coordinate transformation is applied as given by

$$\lambda \to a\zeta \tag{6.33}$$

by which Equation 6.30 transforms to[8]

$$\frac{\partial^2\psi}{\partial\zeta^2} + \frac{2}{\zeta}\frac{\partial\psi}{\partial\zeta} = a^2\phi_1^2\psi\exp\left(\beta\gamma\frac{1-\psi}{1+\beta\,(1-\psi)}\right). \tag{6.34}$$

This transformation makes it possible to convert the boundary value problem into an initial value problem. The strategy to solve Equation 6.34 is by setting a value for $a^2\phi^2$ and **assuming** a value for ψ at $\zeta = 0$. That is, the dimensionless concentration at the center of the particle is set to a value of our choice. Next, Equation 6.34 is integrated until $\psi = 1$ is found and we make note at which value for ζ this happens. To comply with Equation 6.31 of the original boundary value problem, $\psi = 1$ should be found when $\lambda = 1$.[9] Observe now that a basically acts as a scaling parameter and by adjusting the value for a, we can ensure that $\psi|_{\lambda=1} = 1$ via

$$a = \frac{1}{\zeta|_{\psi=1}}. \tag{6.35}$$

The key idea is thus that rather than solving the boundary value problem, we simply choose a concentration ψ at $\lambda = 0$ and then determine the value of ϕ this would give by ensuring that $\psi|_{\lambda=1} = 1$. In other words, one "shoots" out trajectories[10] from one boundary until we find a trajectory that "hits" the other boundary condition.[5]

To perform the spatial integration, note that the second order differential equation as given by Equation 6.34 can be rewritten as two coupled first-order differential equations as given by

$$\frac{\partial u_1}{\partial\zeta} = u_2 \tag{6.36}$$

$$\frac{\partial u_2}{\partial\zeta} = -\frac{2}{\zeta}u_2 + a^2\phi_1^2u_1\exp\left(\beta\gamma\frac{1-u_1}{1+\beta\,(1-u_1)}\right), \tag{6.37}$$

wherein

$$u_1 = \psi \tag{6.38}$$

$$u_2 = \frac{\partial\psi}{\partial\zeta}. \tag{6.39}$$

There however remains a complexity we have to deal with in order to numerically integrate Equations 6.36 and 6.37. At $\zeta = 0$, the term $\frac{2}{\zeta}\frac{\partial\psi}{\partial\zeta}$ is ill-defined. To resolve upon this, let us perform a Taylor expansion on $\frac{\partial\psi}{\partial\zeta}$, which gives

[8] For clarity, I have expanded the ∇ operator to clearly indicate that the dependent variable has changed from λ to ζ.

[9] The concentration at the surface of the particle should equal the bulk concentration.

[10] If you think about, setting the value for ψ at $\zeta = 0$ determines how the curve is going run. So by setting it, we are aiming our numerical cannon.

$$\frac{\partial \psi}{\partial \zeta} = \left.\frac{\partial \psi}{\partial \zeta}\right|_{\zeta=0} + \zeta \cdot \left.\frac{\partial^2 \psi}{\partial \zeta^2}\right|_{\zeta=0} + \frac{\zeta^2}{2} \cdot \left.\frac{\partial^3 \psi}{\partial \zeta^3}\right|_{\zeta=0} + \frac{\zeta^3}{6} \cdot \left.\frac{\partial^4 \psi}{\partial \zeta^4}\right|_{\zeta=0} \cdots \quad (6.40)$$

Because of symmetry, all the odd terms in ζ will cancel out. If we terminate the series after the quadratic term, we obtain

$$\frac{\partial \psi}{\partial \zeta} = \zeta \cdot \left.\frac{\partial^2 \psi}{\partial \zeta^2}\right|_{\zeta=0}, \quad (6.41)$$

by which we find that

$$\lim_{\zeta \to 0} \left(\frac{\zeta}{2} \frac{\partial \psi}{\partial \zeta} \right) = 2 \left.\frac{\partial^2 \psi}{\partial \zeta^2}\right|_{\zeta=0}. \quad (6.42)$$

Plugging this result back into Equation 6.34 and setting $\zeta = 0$, we find that

$$\left.\frac{\partial^2 \psi}{\partial \zeta^2}\right|_{\zeta=0} = \frac{1}{3} a^2 \phi_1^2 \psi_0 \exp\left(\beta\gamma \frac{1-\psi_0}{1+\beta(1-\psi_0)} \right), \quad (6.43)$$

wherein ψ_0 is the value of ψ at $\zeta = 0$. Consequently, at $\zeta = 0$, we set

$$\left.\frac{\partial u_1}{\partial \zeta}\right|_{\zeta=0} = 0 \quad (6.44)$$

$$\left.\frac{\partial u_2}{\partial \zeta}\right|_{\zeta=0} = \frac{1}{3} a^2 \phi_1^2 \psi_0 \exp\left(\beta\gamma \frac{1-\psi_0}{1+\beta(1-\psi_0)} \right), \quad (6.45)$$

By means of the above recipe, we thus find a Thiele modulus ϕ as function of a starting concentration ψ_0 and by calculating the first derivative of ψ at $\lambda = 1$[11], we can determine the efficiency factor η by means of

$$\eta = \frac{3}{a\phi_1^2} \frac{\partial \psi}{\partial \zeta} \text{ at } \zeta = \frac{1}{\alpha}. \quad (6.46)$$

With this procedure established, we can construct curves of ψ versus η using the following algorithm.

1. Select a list of starting concentrations ψ_0 and a given value of β and γ.
2. Determine by integrating Equations 6.36 and 6.37 the value of ζ at which $\psi = 1$ for each ψ_0 and calculate the value of a from Equation 6.35.
3. Rescale the problem and establish the value of ϕ from a and calculate η from Equation 6.46.
4. Construct the curve of η versus ϕ.

[11] Note that we have direct access to this first derivative as it corresponds to the value of u_2.

It turns out that even with high numerical precision (e.g. 64 bits floating point numbers), there is a limit to what can still be accurately calculated and especially for values of $\phi > 50$, numerical instabilities start to occur. To nevertheless find results up to $\phi = 1000$, Weisz and Hicks proposed to use an extrapolation procedure.[12] I am going to skip on the details of this extrapolation procedure as it can be found in the original work[6] and it does not add to the story. In fact, if you would take a ruler and align it along side the last few points of the curve and extend the line, you would more of less obtain the same result.[13]

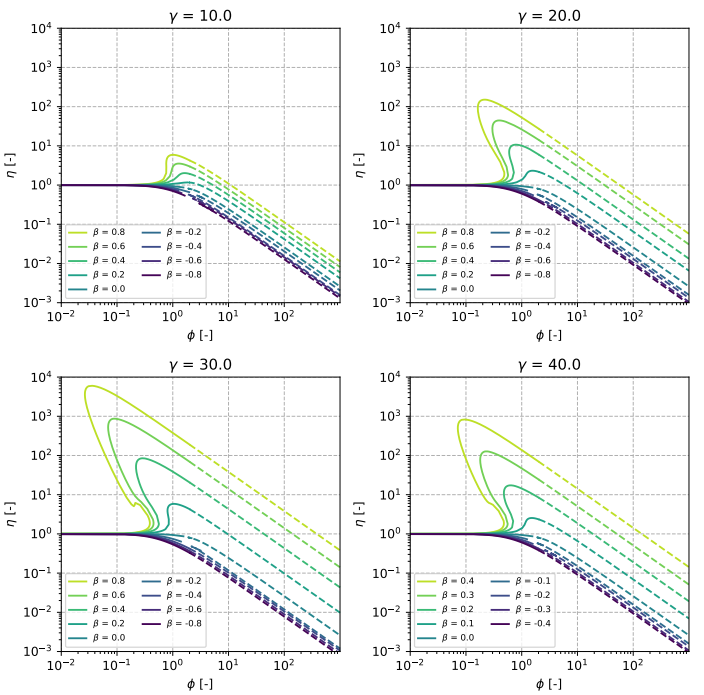

Figure 6.1: *Efficiency η as function of the Thiele modulus ϕ under non-isothermal conditions. The dashed lines corresponds to regions of the curve that are constructed by means of extrapolation.*

In Figure 6.1, the efficiency factor η as function of the Thiele modulus ϕ is depicted for various choices of β and γ. From this figure, it can be readily seen that with increasing value of γ, the efficiency factor of the catalyst for positive values of β rapidly increases and can, in some situations, reach values as large as 10^4. Large values of γ correspond to a high temperature-dependency of the reaction and large values of β correspond to a significant temperature rise. Consequently, when both are high, the particle rapidly increases in temperature which leads to an increased rate of the reaction. Conversely, when γ remains high but β is negative, the reaction is endothermic and the particle cools down as

[12] I would like to emphasize that Weisz and Hicks explicitly mention in their paper that they never performed a formal error analysis on this extrapolation procedure. As such, it is good practice when plotting the ϕ versus η curves to show which part of the curve is explicitly calculated and which part is extrapolated. In this work, I will do so, but plenty of works in the literature find it necessary to ignore upon such details.

[13] Arguably, you would sometimes obtain perhaps an even better result as the extrapolation procedure depends on a fixed interval size.

a result of the reaction. This decrease in temperature leads to reduced rate of chemical conversion and as such, very small efficiency factors are observed.

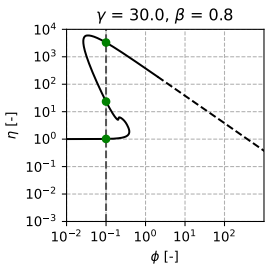

Figure 6.2: *Efficiency factor as function of the Thiele modulus for a dimensionless temperature increase of β of 0.8 and an Arrhenius number γ of 30.0.*

6.4 Stable states and bifurcations

Let us extract one particular scenario from Figure 6.1 wherein $\beta = 0.8$ and $\gamma = 30.0$. From the shape of the curve, it can be established that at least three different efficiency factors are possible for a single value of ϕ. Such a result would imply that the catalyst pellet can operate under multiple working states. These working states are indicated by the green circles in Figure 6.2.

Since a catalyst pellet under steady-state conditions can only exist in a single working state at a given point in time[14], it is interesting to explore what determines in which state the catalyst will operate. Since β and γ as well as the boundary conditions of the problem are fixed, the only remaining determining factor are the initial conditions. Indeed, by *a priori* choosing a value for ψ at $\lambda = 0$, we basically pre-determined in which working state the catalyst particle will operate.

To better understand this process, let us consider the unsteady-state non-isothermal behavior and explore the evolution of the concentration profile in the particle as function of time, given an initial concentration $\vec{\psi}_{\tau=0}$[15] throughout the particle. This initial concentration is set-up as such that it is some constant value $\psi_{\tau=0,\lambda=0} = \psi_0$ at the center of the spherical pellet and $\psi_{\lambda=1} = 1$[16] at the edge. For the values in between, a simple linear interpolation is performed. An example of such a time-evolution of the concentration in the catalyst pellet is shown in Figure 6.3.

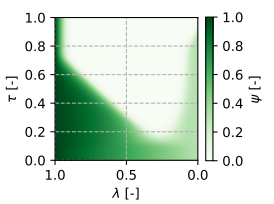

Figure 6.3: *Time evolution of the dimensionless concentration profile. Observe that the initial dimensionless concentration is linearly interpolated between $\psi = 1$ at $\lambda = 1$ and $\psi = \psi_0$ at $\lambda = 0$. The time evolution is shown as function of dimensionless τ which is defined such that $\tau = 1$ upon convergence.*

At each point in time, we can determine the efficiency of such a system on the basis of the concentration profile $\vec{\psi}$. So rather than showing the complete concentration profile for a certain time series as done in Figure 6.3, the profile is essentially condensed to a single number, being the efficiency factor η. Given a starting condition ψ_0, we can now follow the time-evolution of a catalyst pellet through phase space[17] using a single curve which is shown in Figure 6.4.

In the left graph in Figure 6.4, the time-evolution for a series of starting conditions $2 \cdot 10^{-1} \leq \psi_0 \leq 1 \cdot 10^{0}$ are considered. As expected from Figure 6.2, all trajectories move to a stable point in phase space. If we now zoom in and construct a second series of trajectories as shown in right graph of Figure 6.4 between $0.45 \leq \psi_0 \leq 0.55$, a clear pattern emerges wherein the trajectories that start in the left hand side of the graph end up in the high-efficiency point whereas the ones that start on the right hand side, end up in the low-efficiency point.

To determine (roughly) at which point this transition occurs, in Figure 6.5, 101 trajectories between $0.4955 \leq \psi_0 \leq 0.4965$ are visualized. From

[14] Catalyst pellets are macroscopic particle, so no quantum chemical nonsense about superpositions and such.

[15] The vector symbol is there to indicate that the initial conditions correspond to a list of values rather than a single value.

[16] This point corresponds to a boundary condition, so the value at this point is static throughout the time-evolution.

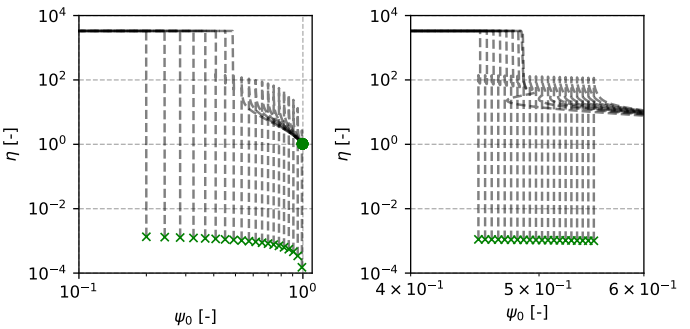

Figure 6.4: *Time-evolution through phase space of the catalyst particle for various starting concentrations ψ_0 for $\gamma = 30$, $\beta = 0.8$, and $\phi = 0.1$. The green crosses are the start points in phase space. Observe that all trajectories end either at $\eta \approx 10^3$ or at $\eta \approx 10^0$. Note that the final point at $\eta \approx 10^3$ corresponds to a ψ_0 of nearly zero and thus lies outside the region of the graph.*

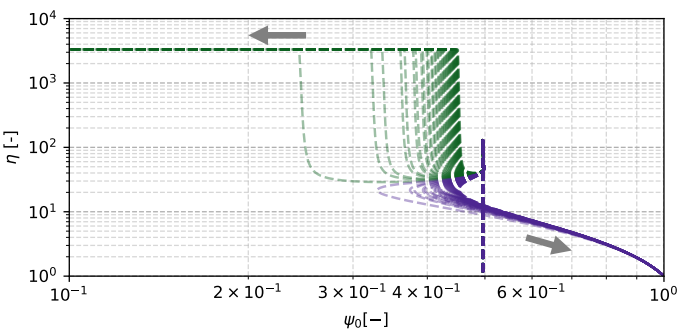

Figure 6.5: *Time-evolution through phase space of the catalyst particle. Only a limited number of trajectories are spawned around the bifurcation point. The green trajectories correspond to a final working state in the high-efficiency region of phase space whereas the purple trajectories correspond to a final working state in the low-efficiency region of phase space.*

Figure 6.5, it can be seen that if the catalyst system is initialized with $\psi_0 = 0.496010\cdots$, then the system will evolve according to the green lines and end up at the high-efficiency point. If we now construct another system with $\psi_0 = 0.496010\cdots + \epsilon$, then for even the smallest values of ϵ, the system will converge to a completely different point in phase space corresponding to a vastly different situation. Such a rapid and sudden transition as function of a single parameter is called a bifurcation and the point at which this occurs is called a **bifurcation point**.

In contrast however to the result as shown in Figure 6.1, the trajectories only end in either the stable point at $\eta \approx 10^3$ or at $\eta \approx 10^0$ but never at the point at $\eta \approx 2 \cdot 10^1$ despite that from Figure 6.1 we would assume

[17] In dynamical system theory, a phase space is a space in which all possible states of a system are represented, with each possible state corresponding to one unique point in the phase space.

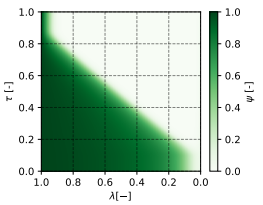

Figure 6.6: *Time evolution of the dimensionless concentration profile using initial conditions corresponding to the point in phase space $\phi_0 = 10^{-1}$ and $\eta \approx 22$.*

[18] This is the center point in Figure 6.1.

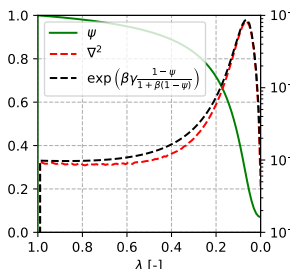

Figure 6.7: *Concentration profile and sink/source terms as function of the dimensionless coordinate λ at $\phi_0 = 10^{-1}$ and $\eta \approx 22$. The solid green line corresponds to the dimensionless concentration. The dashed black line corresponds to the diffusion term, i.e. how much material diffuses into the control volume. The dashed red line corresponds to the reaction term, i.e. how much material is consumed or how much heat is produced.*

[19] The book "Elements of Chemical Reactor Engineering" of H. Scott Fogler[7] discusses in detail about the concept of multiple steady states, both stable and unstable ones. Especially chapter 8 in this book makes an interesting read.

this would also correspond to a valid solution. To understand why this is, let us consider the time-evolution of a system prepared in such a way it corresponds to this intermediary point in phase space.[18] In Figure 6.6, the time-evolution is shown and it can be readily observed that the concentration profile changes and converges to the high-efficiency situation. This leads to the conundrum that one numerical method, i.e. the shooting method, predicts an intermediate operating state of the catalyst while another numerical method, i.e. time-integration, predicts that if we would prepare a catalytic system in this intermediate operating state, it would diverge away from this state.

To understand this discrepancy, we look into the intermediate working state in more detail. The time-evolution of the system is given by

$$\frac{\partial \psi}{\partial t} = \nabla^2 \psi - \phi_1^2 \psi \exp\left(\beta\gamma \frac{1-\psi}{1+\beta(1-\psi)}\right) \tag{6.47}$$

wherein the two terms on the right hand side correspond to a diffusion source term

$$S_{\text{diffusion}} = \nabla^2 \psi \tag{6.48}$$

and to a reaction sink term

$$S_{\text{reaction}} = \phi_1^2 \psi \exp\left(\beta\gamma \frac{1-\psi}{1+\beta(1-\psi)}\right). \tag{6.49}$$

The diffusion source term, ∇^2 corresponds to the influx of material into a given control volume at position λ due to the concentration gradient. The reaction sink term corresponds to the consumption of material by the ongoing reaction. A stable working condition is such the these sink/source terms are balanced and thus of equal magnitude for all control volumes. In Figure 6.7, the concentration profile, the diffusion source term and the reaction sink term are shown. From this figure, it can be seen that for some parts of the catalyst pellets, these terms are not equal in magnitude and as such, the working state is unstable.

The time-integration numerical method obviously catches upon this aspect and because of the discrepancy between the source and sink terms, the system will evolve further over time. In contrast, for the shooting method, it is only verified whether the dimensionless concentration is unity at the cell boundary and this is certainly the case. As such, the intermediate working stable should be interpreted as an **unstable state**. The catalytic system can pass through this state, but can never form a stable working state at this point in phase space.[19]

.

BIBLIOGRAPHY

(1) Janssen, L.; Warmoeskerken, M., *Transport Phenomena Data Companion*; VSSD: 1987; Vol. 1.

(2) Adams, R.; Essex, C., *Calculus: A Complete Course*; Pearson Education: 2021.

(3) Danckwerts, P. *Chemical Engineering Science* **1953**, *2*, 1–13, DOI: https://doi.org/10.1016/0009-2509(53)80001-1.

(4) Weisz, P.; Prater, C. In Frankenburg, W., Komarewsky, V., Rideal, E., Eds.; Advances in Catalysis, Vol. 6; Academic Press: 1954, pp 143–196, DOI: https://doi.org/10.1016/S0360-0564(08)60390-9.

(5) Press, W.; Teukolsky, S.; Vetterling, W.; Flannery, B., *Numerical Recipes: The Art of Scientific Computing*, 3rd; Cambridge University Press: 2007.

(6) Weisz, P. B. *Chemical Engineering Science* **1995**, *50*, 3949–3950, DOI: https://doi.org/10.1016/0009-2509(96)81826-4.

(7) Fogler, H. S., *Elements of Chemical Reactor Engineering*, 4th ed.; Pearson Education: 2006.

.

INDEX